

# Gold Nanoclusters: Imaging, Therapy, and Theranostic Roles in Biomedical Applications

Sanne M. van de Looij,<sup>#</sup> Erik R. Hebels,<sup>#</sup> Martina Viola, Mathew Hembury, Sabrina Oliveira, and Tina Vermonden<sup>\*</sup>



Cite This: *Bioconjugate Chem.* 2022, 33, 4–23



Read Online

ACCESS |

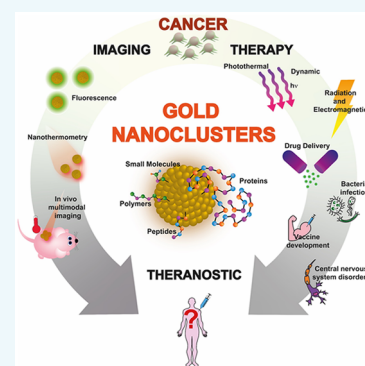


Metrics & More



Article Recommendations

**ABSTRACT:** For the past two decades, atomic gold nanoclusters (AuNCs, ultrasmall clusters of several to 100 gold atoms, having a total diameter of <2 nm) have emerged as promising agents in the diagnosis and treatment of cancer. Owing to their small size, significant quantization occurs to their conduction band, which leads to emergent photonic properties and the disappearance of the plasmonic responses observed in larger gold nanoparticles. For example, AuNCs exhibit native luminescent properties, which have been well-explored in the literature. Using proteins, peptides, or other biomolecules as structural scaffolds or capping ligands, required for the stabilization of AuNCs, improves their biocompatibility, while retaining their distinct optical properties. This paved the way for the use of AuNCs in fluorescent bioimaging, which later developed into multimodal imaging combined with computer tomography and magnetic resonance imaging as examples. The development of AuNC-based systems for diagnostic applications in cancer treatment was then made possible by employing active or passive tumor targeting strategies. Finally, the potential therapeutic applications of AuNCs are extensive, having been used as light-activated and radiotherapy agents, as well as nanocarriers for chemotherapeutic drugs, which can be bound to the capping ligand or directly to the AuNCs via different mechanisms. In this review, we present an overview of the diverse biomedical applications of AuNCs in terms of cancer imaging, therapy, and combinations thereof, as well as highlighting some additional applications relevant to biomedical research.



## 1. INTRODUCTION

For the past few decades, cancer has been a major public health concern, being the second leading cause of mortality worldwide.<sup>1</sup> It has become clear that upon earlier detection of the tumor, the 5-year survival rates of patients are improved.<sup>2,3</sup> Detection and identification of the disease before metastasis are thus critical when treating cancer.<sup>4</sup> Therefore, while priority must be given to providing treatment options for these patients, designing new or improving already existing cancer detection methods is crucial to improve treatment success.

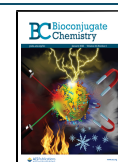
Recently, gold nanoclusters (AuNCs) have emerged as a promising detection approach in biomedical imaging, due to their unique molecule-like properties and good biocompatibility.<sup>1</sup> Gold, as an element in particular, is an attractive inert noble metal with good biocompatibility and substantial history in biomedical applications.<sup>5</sup> AuNCs are ultrasmall clusters of several to 100 gold atoms, having a total diameter of less than 2 nm.<sup>6</sup> As opposed to gold nanoparticles with a diameter larger than 2 nm and having a continuous band of electronic energy, distinct electron excitation levels start to appear when the size of the gold core becomes comparable to the Fermi wavelength of an electron ( $\sim 0.5$  nm).<sup>1,6–9</sup> Because of the quantum confinement effects,<sup>10</sup> significant quantization of the conduction band occurs,<sup>6</sup> and the AuNC can be energetically

considered as a molecule.<sup>1</sup> This leads to unique optical properties such as fluorescence, which is caused by electron transitions between these electron energy levels upon light activation.<sup>4</sup> Considering that AuNCs absorb light in the near-infrared (NIR) range between 650 and 900 nm,<sup>6</sup> they are especially useful in a biological window of cancer diagnostics. NIR light has a tissue penetration between that of optical light and X-rays and is relatively harmless to healthy cells, in contrast to wavelengths that are currently used for medicinal purposes.<sup>11</sup> Besides that, fluorescent probes that emit light in the NIR range have the advantage of having minimum interference from background fluorescence and light scattering in biological systems.<sup>1,12</sup> In addition to their photoluminescence, AuNC-based systems generally also are biocompatible, more photostable than commonly used organic dyes, and possess a large Stokes shift and a long luminescence lifetime.<sup>1,8</sup> By utilizing surface protecting ligands, also known as capping

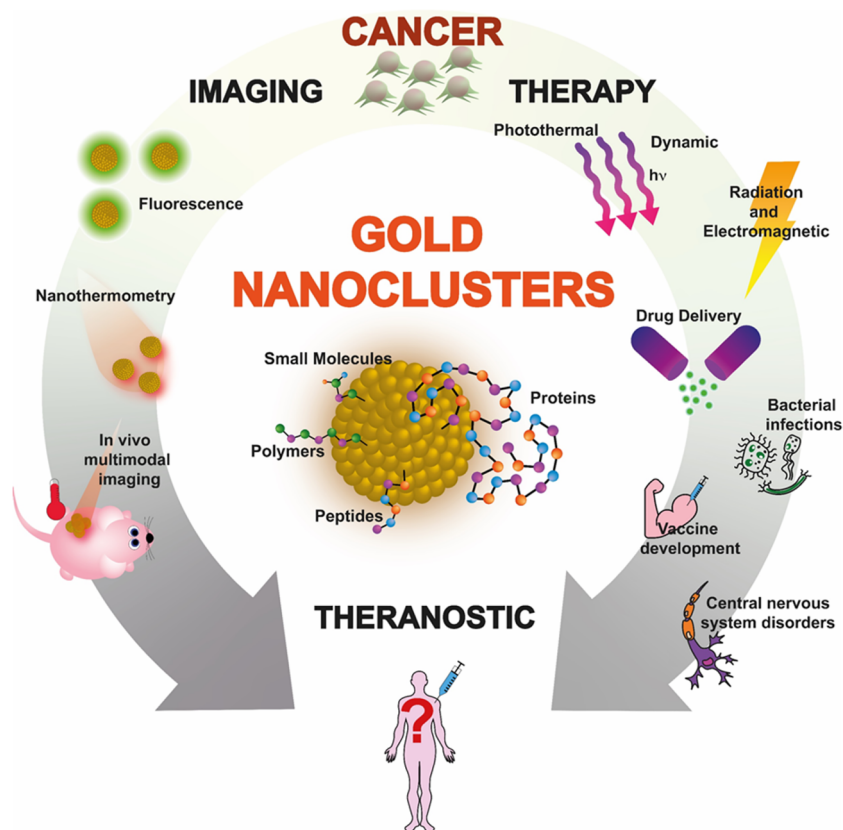
Received: September 30, 2021

Revised: November 25, 2021

Published: December 12, 2021



**Scheme 1. Schematic Illustration of AuNCs with Various Classes of Capping Ligands, Investigated for Potential Use in Imaging, Therapy, and Theranostic Platforms**



ligands, the AuNCs can be stabilized to prevent coalescence.<sup>9</sup> Also, with the help of these ligands, the specific photoluminescent wavelengths can be tuned by adapting either the size or the surface-chemistry of the metal core.<sup>10</sup> By performing reduction of gold in solution in the presence of thiols or macromolecular templating agents, nanocluster and ligands can be covalently bound.<sup>13</sup>

AuNCs are not only applicable as a tool for *in vivo* bioimaging. By conjugating drugs to either the capping ligands or the AuNCs directly, the system can aid in therapy too. Additionally, because of the inherent properties of AuNCs, such as a good photothermal conversion, other types of triggered therapy are also within reach.

Herein, a review regarding cancer nanomedicines with AuNCs is given, a platform where medical imaging and cancer cell-targeted therapy can be integrated. The development of AuNCs over the past few years will be discussed in terms of imaging, therapy, and theranostic applications to provide an overview of research that has been executed thus far. A theranostic system is defined as a material that combines therapy and diagnostic imaging in one platform.<sup>14</sup> They deliver therapeutic drugs or aid in another form of therapy, while also acting as or delivering a diagnostic imaging agent at the same time. Moreover, the potential applications of AuNCs in neurological disorders, antibiotics, and vaccine development will be discussed briefly (Scheme 1), followed by a discussion to determine the knowledge gap and future perspectives.

## 2. AUNCS IN FLUORESCENT BIOIMAGING

Most of the research conducted has focused on using thiols, bovine serum albumin, or glutathione as capping ligands to

obtain stabilized fluorescent AuNCs.<sup>13</sup> However, many different capping ligands have been used in the synthesis to improve the quantum yield of the luminescent emission (QY) or pharmacokinetic factors. The QY of the ligand-protected AuNCs is an essential parameter for the characterization of their light emission properties,<sup>15</sup> where a higher QY is an indication of increased photoluminescent signal. It is the ratio of the amount of photons that are emitted to the amount of photons that are absorbed.<sup>16</sup>

One of the current challenges in the development of AuNCs for bioimaging techniques is that the ligand-protected AuNCs often have a very low QY of less than 1%, limiting their *in vivo* applications.<sup>13</sup> Alongside that, the colloidal stability of the protected AuNCs is usually not optimal either, nor are the biodistribution or clearance and accumulation in target organs.<sup>17</sup> Nevertheless, multiple research groups have aimed to figure out how to adapt the surface-chemistry of the AuNCs to solve all these problems. Wu et al. (2010) found that the most effective strategy to enhance fluorescence from AuNCs is to employ ligands with electron-rich atoms (e.g., N, O, S, P) and groups (e.g., carboxylic acid, amines).<sup>9,10</sup> AuNCs are often developed with polymers as capping ligands or endogenous biomolecules, such as peptides, proteins, and DNA in order to increase their biocompatibility. Table 1 and Table 2 give an overview of some relevant articles for fluorescent bioimaging systems employing AuNCs and additional fluorescent properties of AuNCs, respectively.

**Fluorescence of AuNCs with Different Capping Ligands.** Well-explored are the bovine serum albumin (BSA)-AuNCs, which were first reported by Xie et al. in 2009.<sup>18</sup> They synthesized red emitting BSA-AuNCs ( $\lambda_{em\ max} =$

**Table 1. Overview of Key Properties of the AuNC-Based Systems from the Studies Mentioned in the AuNCs in Fluorescent Bioimaging Section**

reference	capping ligand	additional functionality	excitation/emission	quantum yield	CT/MRI/PET/PAI
Hembury, 2018 <sup>6</sup>	PEG-PNIPAM	-	550/720 nm	3.6%	-
Xie, 2009 <sup>18</sup>	BSA	-	480/640 nm	6%	-
Wang, 2013 <sup>20</sup>	Transferrin	-	380/710 nm	7.7%	-
Chen, 2012 <sup>21</sup>	Lysozyme type VI	-	380/455 nm	56%	-
Wei, 2010 <sup>22</sup>	Lysozyme	-	360/657 nm	7%	-
West, 2014 <sup>27</sup>	Dnase-1	-	460/640 nm	Not reported	-
Wen, 2011 <sup>28</sup>	Horseradish peroxidase	-	365/650 nm	Not reported	-
Li, 2020 <sup>23</sup>	Keratin	Ag ions	470/710 nm	10.5%	-
Kawasaki, 2011 <sup>24</sup>	Pepsin	-	360/670 nm	3.50%	-
Liu, 2011 <sup>25</sup>	Insulin	-	400/670 nm	7%	-
Kong, 2013 <sup>26</sup>	RNase-A	-	470/682 nm	12.1%	-
Chen, 2017 <sup>30</sup>	Zwitterionic/bidentate thiol molecules	-	532/1000–900 nm	0.6–3.8%	-
Lopez, 2015 <sup>31</sup>	DNA	-	560/764 nm	3%	-
Zhou, 2011 <sup>32</sup>	GSH	-	420/560 nm	3.5%	-
Han, 2019 <sup>50</sup>	HSA	Tumor-targeting peptide release hormone, iodine 124	Not reported	Not reported	PET
Zheng, 2004 <sup>35</sup>	PAMAM dendrimer	-	340/380 nm to 760/880 nm	70–10%	-
Santiago González, 2010 <sup>36</sup>	PVP	-	240/350 nm	12.5%	-
Duan, 2007 <sup>37</sup>	PEI	-	353/445 nm	10–20%	-
Hussain, 2005 <sup>38</sup>	Thiol-terminated PMMA	-	Not reported	Not reported	-
Adnan, 2017 <sup>39</sup>	OEGMA-AcSEMA	-	440/640–660 nm	0.24% and 0.17%	-
Al Zaki, 2014 <sup>40</sup>	Polymeric micelle	-	Not reported	Not reported	CT
Chen, 2013 <sup>41</sup>	Polymeric micelle	-	405/610 nm	Not reported	-
Liu, 2013 <sup>47</sup>	Trypsin	Folic acid	520/690 nm	6.5%	-
Zhang, 2014 <sup>48</sup>	BSA	Folic acid or Hyaluronic acid	370 or 470/600 nm	~15%	-
Liu, 2016 <sup>51</sup>	Lysozyme	Folic acid	550/690 nm	19.61%	CT
Hu, 2013 <sup>52</sup>	None	Gadolinium ions	435–480/600–800 nm	Not reported	CT, MRI
Hembury, 2015 <sup>49</sup>	Mesoporous silica shells	Gold nanoparticles	680/800–860 nm	0.02%	MRI, PAI
Liu, 2019 <sup>43</sup>	GSH	Doped nanocluster	808/1300–1700 nm	0.67% (Cu-doped)	-

640 nm) with QY of approximately 6%. However, later research found an unsatisfying colloidal stability and biodistribution,<sup>17,19</sup> providing challenges for *in vivo* applications. Yet, BSA-templated AuNCs have been extensively studied in the context of targeting and drug delivery,<sup>13</sup> considering their ability to be functionalized with targeting molecules such as the monoclonal antibody herceptin or the synthetic vitamin folic acid. BSA is not the only protein that has been investigated as a template for AuNC synthesis. Also, transferrin ( $\lambda_{em\ max} = 710\ nm$ , QY = 7.7%),<sup>20</sup> lysozyme type VI ( $\lambda_{em\ max} = 455\ nm$ , QY = 56%),<sup>21</sup> lysozyme ( $\lambda_{em\ max} = 657\ nm$ ),<sup>22</sup> keratin-Ag ( $\lambda_{em\ max} = 710\ nm$ , QY = 10.5%),<sup>23</sup> pepsin ( $\lambda_{em\ max} = 670\ nm$ , QY = 3.5%),<sup>24</sup> insulin ( $\lambda_{em\ max} = 670\ nm$ , QY = 7%),<sup>25</sup> RNase-A ( $\lambda_{em\ max} = 682\ nm$ , QY = 12.1%),<sup>26</sup> DNase 1 ( $\lambda_{em\ max} = 640\ nm$ ),<sup>27</sup> horseradish peroxidase ( $\lambda_{em\ max} = 650\ nm$ ),<sup>28</sup> ovalbumin, urease, and immunoglobulin G have been investigated as a template for AuNC synthesis, among others. In these studies, different sizes of AuNCs were employed, so part of the differences in fluorescent properties can be attributed to that variable. On several occasions, it was shown that the proteins kept their endogenous functions even after the AuNC synthesis.<sup>26,27</sup>

Xu et al. performed a systematic review in which they determined the influence of the protein templates on the AuNC fluorescence, based on the protein characteristics.<sup>29</sup> It

was found that protein templates with many cysteine residues cause a shift in the fluorescent emission to higher wavelengths (red shift). They also appear to cause shorter fluorescent lifetimes.<sup>29</sup>

By making use of zwitterionic and bidentate thiol molecules as capping ligands, Chen et al. (2017) have reported short wavelength infrared (SWIR,  $\lambda = 1\text{--}2\ \mu\text{m}$ ) emitting AuNCs with a QY of 0.6% to 3.8% for emission wavelengths between 1000 and 900 nm, respectively.<sup>30</sup>

DNA-templated AuNC synthesis has also been performed.<sup>31</sup> The emission color of the AuNCs is mainly dependent on the degree of metal reduction, while the DNA sequence and chain length only play a minor role in the specific fluorescent emission. An optimized process yielded AuNCs with a QY of about 3%.<sup>31</sup>

The tripeptide glutathione (GSH) has been commonly used as a AuNC surface ligand because of its limited interaction and affinity to cellular proteins.<sup>1</sup> It has been found that glutathione reduces the accumulation of AuNCs in the liver and the spleen, while improving renal clearance, leading to at least 50% of GSH-coated AuNCs to be effectively removed from the body via the urinary systems within 24 h after IV-injection.<sup>32</sup> Zhou et al. reported a QY of 3.5% and a photoluminescence in the NIR range of approximately 560 nm.<sup>32</sup> In addition to this, the findings of Luo et al. in 2012<sup>33</sup> showed that in the context of

Table 2. Overview of Key Properties of the AuNC-Based Systems from the Studies Mentioned in the Additional Fluorescence-Based Applications of AuNCs Section

ref	capping-ligand	other functionality	excitation/ emission	QY	application	result
Wang, 2018 <sup>19</sup>	Keratin	Ag ions	400/725 nm	10.7%	Sensing mercury(II)	Lower limit of detection of 2.31 nM
Liu, 2013 <sup>47</sup>	Trypsin	Folic acid	520/690 nm	6.5%	Sensing heparin	Lower limit of detection 0.05 $\mu\text{g/mL}$ , sense heparin in human serum with a linear range between 0.1 and 4.0 $\mu\text{g/mL}$
Zhang, 2019 <sup>53</sup>	GSH	-	430/610 nm	Not reported	Temperature sensing	Temperature resolution of 0.73 $^{\circ}\text{C}$ in hepatic stellate cells between 35 and 43 $^{\circ}\text{C}$
Yang, 2019 <sup>54</sup>	PAMAM dendrimer	-	390/453 nm	18%	Temperature sensing, sensing dichromate	Distinguish temperature in the range of 15 to 80 $^{\circ}\text{C}$ . Lower limit of detection of 1.9 $\mu\text{M}$
Shang, 2013 <sup>55</sup>	Lipoic acid	-	580/710 nm	Not reported	Temperature sensing	Temperature resolution between 0.3 and 0.5 $^{\circ}\text{C}$ in HeLa cells between 15 and 45 $^{\circ}\text{C}$ .
Selvaprakash, 2014 <sup>58</sup>	Chicken egg ovalbumin	-	370/640 nm	6.6%	Sensing ATP and pyrophosphate	Lower limit of detection ATP 19 $\mu\text{M}$ , lower limit of detection pyrophosphate 5 $\mu\text{M}$
Xia, 2013 <sup>59</sup>	Glucose-oxidase	-	507/650 nm	~7%	Sensing of Glucose	Lower limit of detection of 0.7 $\mu\text{M}$ within a linear range between 2.0 and 140 nM
Peng, 2012 <sup>60</sup>	Calcium carbonate	Horseradish peroxidase/ antibody conjugates	Not reported/ 605 nm	Not reported	Sensing neuron-specific enolase	Lower limit of detection 2.0 pg/mL via fluorescent detection.
Govindaraju, 2017 <sup>61</sup>	BSA	-	450/650 nm	~8%	Sensing dopamine in the cerebrospinal fluid	Lower limit of detection 0.830 nM in cerebrospinal fluid. Linear range between 0 and 10 nM
Yang, 2013 <sup>62</sup>	Poly diallyldimethyl ammonium chloride/Boron nitride	-	405/565 nm	Not reported	Sensing interleukin-6	Lower limit of detection 0.03 ng/mL, with a logarithmic range between 0.1 and 500 ng/mL
Liu, 2017 <sup>63</sup>	Peptide (NH <sub>2</sub> -CCYLRRASLG-COOH)	-	330/405 nm	Not reported	Sensing activity protein kinase A	Lower limit of detection 0.02 U/mL. Activity of protein kinase A can be detected in the range between 0.05 and 1.6 U/mL activity



GSH-Au complexes, a lower ratio of thiol-to-gold (1.5:1 instead of 2:1) and controlled aggregation by solvent mixing in the synthesis of AuNCs can lead to a higher QY of around 15%.<sup>13,33</sup> Metal nanocluster aggregation induced emission is a now a promising and well-recognized phenomenon, providing efficient syntheses of highly luminescent nanoclusters. For a detailed review of aggregation induced emission of metal nanoclusters, the reader is referred to Bera et al.<sup>34</sup>

In 2004, Zheng et al. discovered a synthesis for highly fluorescent, water-soluble, and size-tunable AuNCs using poly(amidoamine) (PAMAM) dendrimers.<sup>35</sup> They found a way to encapsulate the AuNCs with different sizes with PAMAM dendrimers to obtain a new platform for *in vivo* applications. The nanoclusters were reported with well-defined excitation and emission spectra ranging from UV to NIR, with QYs between 70% and 10%, respectively, depending on the size of the gold clusters.<sup>35</sup> Since then, more research has been done with polymers or dendrimers as templates for AuNCs, using poly(*N*-vinylpyrrolidone) (PVP),<sup>36</sup> polyethylenimine (PEI),<sup>37</sup> or thiol-terminated PMMA (poly(methyl methacrylate)) polymers.<sup>38</sup> More recently, an approach was described using copolymers comprising oligo(ethylene glycol) methyl ether methacrylate (OEGMA) and 2-(acetylthio)ethyl methacrylate (AcSEMA) monomers.<sup>39</sup> Hembury et al. combined AuNCs and thermosensitive diblock copolymers consisting of poly(ethylene glycol) (PEG) and poly(*N*-isopropylacrylamide) (PNIPAM)<sup>6</sup> and obtained a QY of 3.6% at a maximum emission wavelength of 720 nm.

Not only polymers but also polymeric micelles have been explored as possible encapsulation scaffolds for AuNCs. Because of their ability to encapsulate other compounds besides the AuNCs, polymeric micelles are usually investigated as theranostic systems. In terms of imaging, Al Zaki et al. investigated gold-loaded polymeric micelles for computed tomography (CT) imaging.<sup>40</sup> They synthesized polymeric micelles consisting of the amphiphilic diblock polymer poly(ethylene glycol)-*b*-poly( $\epsilon$ -caprolactone). The AuNCs were encapsulated within the hydrophobic core of these micelles. Whereas the CT imaging capabilities of the micelles were investigated, the fluorescent properties were not investigated at all.<sup>40</sup> This is in contrast to the research of Chen et al. in 2013, where the fluorescence of the amphiphilic gold-loaded polymeric micelles was investigated ( $\lambda_{em} = 610$  nm).<sup>41</sup>

Imaging in the near-infrared II (NIR-II) region of between 1100 and 1700 nm is attracting wide interest due to reduced tissue scattering as compared to the NIR-I region (750–900 nm).<sup>42</sup> In line with this, Liu et al. in 2019<sup>43</sup> synthesized atomically precise GSH capped Au<sub>25</sub> clusters that emit fluorescence between 1100 and 1350 nm by charge transfer between GSH and the gold core. Metal doping of these AuNCs, with copper for example, increases the QY up to 5-fold. *In vivo* imaging of primary and even metastatic tumors following IV injection of these AuNCs could be performed in mice with excitation at 808 nm and emission of 1300–1700 nm. Cerebral blood vessel imaging was possible as well due to the long wavelength emission in this NIR-II region which allows penetration of the skull.<sup>43</sup>

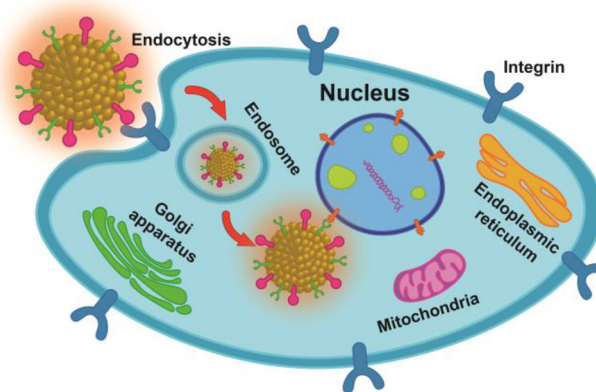
**AuNCs in *In Vivo* Multimodal Bioimaging.** The applicability of AuNCs and hybrid materials including AuNCs as tumor imaging agents has been investigated *in vivo* involving techniques such as X-ray computed tomography, NIR fluorescent imaging, positron emission tomography

(PET), and magnetic resonance imaging (MRI).<sup>1,44</sup> Each imaging technique has its own advantages and disadvantages. Multimodal imaging is a combination of multiple imaging techniques, combining the best features of each. Having a single imaging agent that could be used for multiple imaging techniques therefore gives advantages over imaging with one technique alone. When imaging for cancer diagnostics, the amount of imaging agent that accumulates in the tumor should be high compared to other organs. The platform should, therefore, target the tumor, via either passive or active targeting.

Passive targeting is done by exploiting the enhanced permeability and retention (EPR) effect, a process that occurs in regions of the body with a high degree of hypoxia and/or inflammation. Both are typical for the tumor microenvironment.<sup>45,46</sup> The tumor vasculature has several abnormalities due to their rapid and disordered growth, resulting in gaps in the endothelium, which provide an opportunity for AuNC containing nanoparticle platforms ranging from 10 to 500 nm in the blood serum to extravasate into the tumor tissue.

Active targeting can be achieved by conjugating targeting ligands to the nanoclusters, to obtain cellular uptake via receptor mediated endocytosis as illustrated in Scheme 2.

#### Scheme 2. Schematic Illustration of Receptor Mediated Endocytosis of Active Targeted AuNCs



Examples of targeting ligands are folic acid (FA), hyaluronic acid (HA), methionine, or cyclic RGD.<sup>1</sup> By employing active targeting, there is an altered biodistribution with a possible higher tumor uptake, causing a strong fluorescent signal for tumor sites *in vivo*. This was demonstrated by several studies, such as that by Liu et al., who showed that folic acid functionalized, trypsin-protected AuNCs (FA-try-AuNCs) could be used for *in vivo* imaging in mice.<sup>47</sup> The FA-try-AuNCs were injected intratumorally in nude mice bearing HeLa tumors of 8 mm. The NIR fluorescent signal in the tumors was detectable immediately from injection and up to 12 hours after injection. In subcutaneously injected healthy control mice, the fluorescent signal could be seen spread over the entire body 5 min post-injection, which disappeared slowly after 12 hours, indicating metabolism and degradation of the AuNCs. A final experiment showed that upon subcutaneous injection, the tumor site was visible after 30 min, although it was less clear than when injection happened intratumorally (Figure 1).<sup>47</sup>

BSA-stabilized AuNCs coated with FA or HA showed similar fluorescent properties *in vivo* and accumulated in either

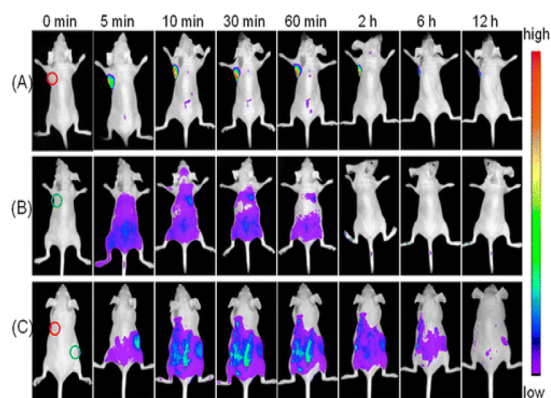


**Figure 1.** *In vivo* time-dependent tumor imaging by NIR fluorescence imaging. The FA-try-AuNCs were injected (A) intratumorally in HeLa tumor-bearing mice, and subcutaneously into the left forelimb region of (B) normal nude (control) mice and (C) tumor-bearing mice. The red circle and green circle indicate the tumor site and injection site, respectively. Reproduced from ref 47. Copyright (2013), American Chemical Society.

HeLa or Hep-2 tumors, respectively.<sup>48</sup> Gadolinium-functionalized AuNCs can generally be used for MRI. Gold-silica quantum rattles (mesoporous silica nanoparticles filled with both AuNCs and gold nanoparticles) have also been reported for multimodal imaging involving MRI.<sup>49</sup> Dependent on the other modifications or conjugations to the AuNC, NIR fluorescent imaging, and CT imaging can also be performed.<sup>1</sup> The shortwave infrared emitting AuNCs that Chen et al. synthesized showed great potential for *in vivo* imaging with a higher contrast than conventional NIR imaging, while also allowing for PET-scans.<sup>30</sup> Additionally, by coupling iodine-124 to a peptide protected AuNC, as done by Han et al. in 2019, the obtained system could be used for PET and fluorescent dual-imaging in lung cancer.<sup>50</sup> They reported the production of these AuNCs by conjugating the tumor-targeting peptide luteinizing hormone releasing hormone to human serum albumin (HSA), and using this as a template for AuNC synthesis.<sup>50</sup>

The lysozyme-capped AuNCs that were designed by Liu et al. in 2016 show great promise for diagnostic purposes.<sup>51</sup> By making use of bimodal bioimaging consisting of NIR fluorescence and CT imaging *in vivo*, cancer tissue and healthy tissues can be distinguished more easily. They found that by adding folic acid as a targeting agent to the lysozyme-capped

AuNCs, they accumulated in the tumor site of HeLa tumor-bearing mice following IV administration.<sup>51</sup> When not using the folic acid modification, the fluorescence of the AuNCs did not appear at the tumor site. When injecting the AuNCs for the purpose of CT imaging, positive signal enhancements could be seen in the liver and kidney one hour after injection, meaning that the AuNCs mainly accumulate in these organs in the absence of tumor tissue.<sup>51</sup>

In 2013, Hu et al. even managed to develop gold-gadolinium nanoclusters for high-performance triple-modal imaging with NIR fluorescence, CT, and MR imaging in a single agent *in vivo*.<sup>52</sup> While doing *in vitro* research, they found that at a concentration as low as 2.1  $\mu\text{M}$ , the hybrid nanoclusters exhibited remarkable signals for NIR fluorescence, CT, and MRI. This triple-modal contrast agent capability was further tested in MCF-7 tumor-bearing mice, where the *in vitro* results were confirmed. The gold-gadolinium nanoclusters also showed a high tumor accumulation and quick renal clearance *in vivo*.<sup>52</sup> Another triple-modal imaging platform was described in 2015 by Hembury et al. utilizing the aforementioned gold-silica quantum rattles. In this case, NIR, MR, and photoacoustic imaging (PAI) could be performed using this single agent in *in vitro* and *in vivo* settings.<sup>49</sup>

**Additional Fluorescence-Based Applications of AuNCs.** The photoluminescent properties of AuNCs have been researched not only in the context of NIR, CT, and MR imaging, but also in diagnostics via nanothermometry or biosensing of heavy metals, small biomolecules, proteins, and cancer biomarkers.

The intracellular temperature is an important parameter in most cellular activities, including gene expression, cell division, and metabolism.<sup>53,54</sup> When abnormal processes occur within the cell, such as cancer cell growth or inflammation, this may result in intracellular temperature changes.<sup>53</sup> AuNCs can be used as intracellular nanothermometers because of the high temperature-sensitivity of their fluorescence lifetime and emission intensity.<sup>55</sup> It was found that both of these factors change drastically within a physiologically relevant temperature range of 15 to 45  $^{\circ}\text{C}$ .<sup>53,55</sup> By making use of fluorescence lifetime imaging microscopy (FLIM), the thermometric properties of AuNCs were tested on several occasions.<sup>53–55</sup> In 2013, Shang et al. used lipoic-acid protected AuNCs to show that the fluorescent emission intensity and fluorescence lifetime both have a negative linear relationship with

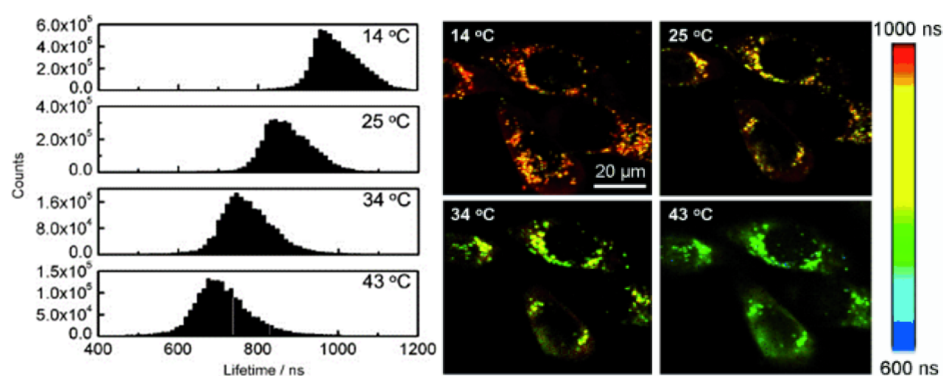


**Figure 2.** *In vitro* fluorescent imaging of AuNCs by making use of fluorescence lifetime imaging. Left: Average lifetime histograms of intracellular gold nanoclusters at varying temperatures. Right: FLIM images of HeLa cells with internalized AuNCs at varying temperatures. Adapted with permission from ref 55. Copyright (2013), John Wiley and Sons.

**Table 3. Overview of Key Properties of the AuNC-Based Systems from the Studies Mentioned in the Sections: AuNCs as a Tool in Therapy, AuNCs Employed in Theranostic Platforms, and AuNCs for Other Biomedical Applications**









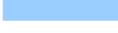
Reference	Capping ligand	Targeting ligand	Disease type	Function AuNCs	Excitation/emission wavelength	Drug-delivery	Linker/Interaction	Specifics	Results
Liu, 2019 <sup>72</sup>	Captopril		Cutaneous squamous cell carcinoma	Photodynamic therapy and Photothermal therapy				NIR laser 808 nm	Photothermal conversion of 41%,
Liu, 2017 <sup>80</sup>	PAMAM-NH <sub>2</sub>		Lung cancer	Alleviate hypoxia for photodynamic therapy				532 nm laser, power density 200 mW/cm <sup>2</sup> PDT with photosensitizer	Reduced hypoxic conditions in tumour tissue improved photodynamic therapy efficacy with statistical significance.
Cifuentes-Rius, 2017 <sup>87</sup>	BSA		Six mammalian cell-lines	Electromagnetic radiation therapy				8 minutes, 15W, 1 GHz electro-magnetic fields	Death in six types of mammalian cells via apoptosis and necrosis at 50 µg/mL AuNCs
Ghahremani, 2018 <sup>86</sup>	BSA	AS1411 aptamer	Breast cancer	Megavoltage radiation therapy				0, 2, 4, 6 Gy gamma rays tested	Factor 2.7 enhanced radiation therapy
Zhang, 2014 <sup>43</sup>	GSH		Cervical cancer	Radiotherapy				5 Gy gamma-rays from 137Cs (photon energy 662 keV) with an activity of 3600 Ci	Enhanced radiosensitivity of 30%, possibly due to higher cell-uptake, after 20 days 35% smaller tumour volume compared to radiation alone
Zhang, 2014 <sup>43</sup>	BSA		Cervical cancer	Radiotherapy				5 Gy gamma-rays from 137Cs (photon energy 662 keV) with an activity of 3600 Ci	Enhanced radiosensitivity of 21%, no significant tumour volume reduction compared to radiation alone
El-Mageed, 2020 <sup>94</sup>	D-penicillamine		Cancer	Drug delivery		D-penicillamine	Interactions: Au-O/S/N bond, hydrogen and electrostatic bond	Calculated <i>in silico</i>	Calculated the interactions and binding energies between D-penicillamine and gold nanoclusters.
Latorre, 2019 <sup>92</sup>	BSA		Breast and pancreatic cancer	Drug delivery		DOX and SN38	pH- or redox-sensitive	Conjugation to BSA by disulphide and maleimide linkers	Enhanced cytotoxicity, leads to apoptosis. Also effective against cancer stem cells
Govindaraju, 2019 <sup>88</sup>	BSA		Lung cancer	Drug delivery	550/650 nm	Kaempferol	Physical interactions		No cytotoxicity in healthy human kidney cells, cytotoxic in lung cancer cells
Lakshmi, 2019 <sup>91</sup>	BSA		Lung cancer	Drug delivery (fluorescence not tested in cells)	360/568 nm	Quercetin	Au-OH interaction		Good cellular uptake and bioimaging properties. High cytotoxicity in lung cancer cells, minimal death in normal fibroblast cells.
Lei, 2017 <sup>99</sup>	GSH-oligoarginine		Pancreatic cancer	Improving stability and circulation time	430/596 nm	NGF siRNA	Adsorbing electrostatic interaction	Loading capacity of 226 µmol siRNA per g GNC	Target tumour-neuron interaction by silencing NGF gene successful
Hebels, 2021 <sup>11</sup>	PEG-PNIPAM core-crosslinked polymeric micelles		Breast Cancer	Triggered drug delivery by NIR light activation	550/720 nm	DOX-SH	Au-S bonds		Highly localized cytotoxicity on MDA-MB-231 cells upon 650 nm light activation
Chen, 2012 <sup>95</sup>	BSA-GPPS	Folic acid	Cervical cancer	Fluorescent imaging	480/620 nm	Camptothecin	Encapsulated		Empty nanocarriers had mild cytotoxicity in HeLa cells
Croissant, 2016 <sup>97</sup>	BSA		Ovarian and breast cancer	Fluorescent imaging	??/645 nm	Gemcitabine and doxorubicin	pH sensitive	Mesoporous silica nanoparticle	Accumulated in kidney and liver
Muthu, 2015 <sup>96</sup>	TPGS micelle	Transferrin	Breast cancer	Fluorescent imaging	365/620 nm	Docetaxel	Encapsulated in lipophilic core		IC50 value up to 72-fold lower than FDA-approved docetaxel formulation.
Jiang, 2020 <sup>100</sup>	GSH		Breast cancer	Photothermal therapy				Indocyanine green as NIR fluorescent dye	The AuNCs managed to completely eradicate tumours
Chen, 2016 <sup>98</sup>	L-histidine	Cyclic RGD and AS1411 aptamer	Malignant glioma	Drug delivery		Doxorubicin	Covalent bond between amine DOX and activated carboxyl group of histidine	Near-infrared dye for fluorescent imaging	Drug release profile not reported
Jiang, 2020 <sup>100</sup>	GSH		Breast cancer	Drug delivery, enhance photothermal therapy, improve stability and circulation time	760/825 (ICG)	Indocyanine green (ICG)	Covalent bond via NHS/amine coupling between GSH and ICG	<i>In vivo</i> : 808 nm NIR laser, 0.8 W/cm <sup>2</sup> power density for 8 minutes	14 days after PTT, breast cancer tumours disappeared for mice treated with ICG-GSH-AuNCs. Free ICG and PBS in combination with PTT showed to therapeutic efficacy.
Luo, 2019 <sup>84</sup>	CY	PSMA	Prostate cancer	Fluorescent imaging, CT imaging and Radiotherapy	490/700 nm				Functional in PSMA positive and PSMA negative tumours
Al Zaki, 2014 <sup>40</sup>	Polymeric micelles		Fibrosarcoma	CT imaging and radiotherapy				6 Gy X-ray radiation	Radiosensitisation of about 1.2, Kaplan-Meier survival curve shows improved survival
Wang, 2020 <sup>104</sup>	PTEN		Liver cancer	Fluorescent imaging and Act as a drug	490 nm			<i>In situ</i> biosynthesis after injection of HAuCl <sub>4</sub> and PTEN DNA	PTEN-AuNC complexes can inhibit or even prevent liver tumour proliferation, invasion and metastasis
Govindaraju, 2018 <sup>89</sup>	BSA and curcumin		Cervical cancer	Fluorescent imaging and drug delivery	550/650 nm	Curcumin	Capping ligand		No cytotoxicity in mortal cell lines, high lethality in human cervical cancer cells
Fu, 2018 <sup>80</sup>	BSA		Neuroblastoma	Fluorescent imaging and drug delivery	510/634 nm	Curcumin	Encapsulated		Higher inhibition efficiency compared to free curcumin or BSA-AuNCs alone
Zhou, 2016 <sup>101</sup>	BSA	Folic acid	Metastased breast cancer	Fluorescent imaging and drug delivery	415/670 nm	Cisplatin	Redox-sensitive		Did not accumulate in healthy organs
Khandelia, 2015 <sup>102</sup>	BSA		Cervical cancer	Fluorescent imaging and drug delivery	505/655 nm	Doxorubicin	Electrostatic interactions and hydrogen bonding	Encapsulation efficiency 83.05%	Lower cytotoxicity than free DOX, possibly due to incomplete release
Kumar, 2018 <sup>103</sup>	Thiol mesoporous silica		Tamoxifen resistant breast cancer	Fluorescent imaging and drug delivery	530/670 nm	EGCG and Vandetanib	Vandetanib bound to Au, EGCG encapsulated in silica	Inhibition of EGFR, VEGFR and AKT pathway	Tumour growth was slowed down
Wang, 2019 <sup>106</sup>	None		Liver cancer	Fluorescent imaging, act as a drug	Confirmed <i>in vivo</i>			<i>In situ</i> biosynthesis after injection of HAuCl <sub>4</sub>	After 38 days reduced tumour growth, reduces signalling in PI3K-AKT pathway
Chen, 2018 <sup>79</sup>	HSA-CAT		Breast cancer	Fluorescent imaging and Photodynamic therapy	365/600-650 nm			NIR-II light excitation 1064 nm for 20 minutes	Due to the CAT functionality, hypoxia was alleviated, PDT is possible
Yang, 2019 <sup>105</sup>	GSH	Hyaluronic acid	Lung cancer	Fluorescent imaging and Photodynamic therapy	580/675 nm	5-fluorouracil	Light/enzyme triggered	Conjugation to graphene, also PTT at 638 nm	Controlled fluorescence and PDT. Light- and enzyme triggered drug release, PTT due to graphene
Liang, 2017 <sup>81</sup>	RGD peptide	RGD peptide	Breast and cervical cancer	Fluorescent imaging, CT imaging and radiotherapy	488/660 nm			6 Gy X-ray radiation at 160 kVp	Tumours only increased 30% in volume compared to 130% for radiation alone
Li, 2020 <sup>23</sup>	Keratin		Breast cancer	Fluorescent imaging, MRI, drug delivery	525/710 nm	Doxorubicin	Redox-sensitive	Gadolinium and silver ions for MRI and enhanced fluorescence	Significant reduction of tumour growth, enhanced fluorescent intensity, biocompatibility and colloid stability, NIR fluorescence
Fernández, 2015 <sup>107</sup>	zwitterionic ligand		Vaccines	DC maturation					Zwitterionic AuNCs cause T helper 1 regulatory cell responses in the form of cytokines, while not leading to proliferation of NK cells and cytotoxic T cells
Tao, 2014 <sup>108</sup>	CpG-ODN-Ovalbumin		Vaccines	Fluorescent imaging, delivery of antigen and adjuvant	490/595 nm				Secretion of TNF-alpha and IL-6 release, gold nanoclusters cause maturation of APCs. Mice developed enhanced anti-ovalbumin IgG response
Tao, 2015 <sup>109</sup>	Thiolated CpG-ODN-Ovalbumin peptide		Vaccines	Fluorescent imaging, delivery of antigen and adjuvant	500/600 nm				CpG-ODN-AuNCs can promote cross-presentation by simultaneous delivery of antigen and adjuvant
Wang, 2016 <sup>110</sup>	HEVA		Hepatitis E Vaccines	Fluorescent imaging, improve immune response and safety profile	365/410 nm		Bonds between Au and cysteine or histidine		Improved safety profile and immunotherapy efficacy <i>in vivo</i> by influencing a Th1/Th2 response.



Table 3. continued

Reference	Capping ligand	Targeting ligand	Disease type	Function AuNCs	Excitation/emission wavelength	Drug-delivery	Linker/Interaction	Specifics	Results
Zheng, 2017 <sup>112</sup>	6-mercapto-hexanoic acid		Bacterial infection	Act as a drug					Can kill both gram-positive and gram-negative bacteria. IC50 against <i>S. aureus</i> comparable with ampicillin and penicillin
Xie, 2020 <sup>111</sup>	DNase		Bacterial infection	Photodynamic therapy and Photothermal therapy				NIR laser 808 nm	Photothermal conversion of 6.59% - Kills 90% of biofilm-shielded bacteria
Xie, 2018 <sup>113</sup>	GSH	QA	Bacterial infection	Act as a drug	362/592 nm		Au-S bonds	<i>In vivo</i> concentration of 40 mg/kg	Comparable with vancomycin in terms of time-kill kinetics and dose-dependent inhibition of <i>S. aureus</i> . Has a broader antibacterial spectrum, including VRE and MRSA
Xie, 2020 <sup>114</sup>	GSH	QA	Prevention of bacterial infection	Act as a drug	360/610 nm		Au-S bonds, electrostatic interaction between AuNC and aligners		Able to prevent biofilm formation in the oral cavity by absorbing on the Invisalign aligners. Active against <i>S. aureus</i> , <i>S. mutans</i> and other gram-positive bacteria.
Ndugire, 2021 <sup>115</sup>	Phosphine and glycosyl ligands	Glycans	Bacterial infection	Act as a drug	Not reported		Au-S and Au-P bonds		Increased bactericidal activity against <i>P. aeruginosa</i> and reduced cytotoxicity to A549 cells as compared to Auranofin (gold (I) analogue)
Xiao, 2020 <sup>116</sup>	Dihydroliipoic acid		CNS disorders	Fluorescent imaging and neuroprotection	405/685 nm				Gold nanoclusters can penetrate the blood-brain barrier
Gao, 2019 <sup>117</sup>	L-NIBC		Parkinson's Disease	Act as a drug					Neuroprotective effect in PD mouse model, prevent aggregation and fibril formation of alpha-synuclein

Colours are based on the categories the AuNC based systems fall in:

	Photothermal and photodynamic therapy
	Radiation and electromagnetic therapy
	AuNCs as a tool in drug delivery
	Theranostic systems employing AuNCs for imaging
	Theranostic systems employing AuNCs for therapy
	Theranostic systems employing AuNCs for imaging and therapy
	AuNCs in vaccine development
	AuNCs in the prevention and treatment of bacterial infection
	AuNCs in central nervous system disorders

temperature between 15 and 45 °C.<sup>55</sup> They showed a temperature resolution between 0.1 and 0.3 °C in phosphate buffered saline (PBS), and between 0.3 and 0.5 °C in HeLa cells (Figure 2). Even temperature differences between subcellular locations could be identified.<sup>55</sup> Similar results were reported for glutathione-capped AuNCs by Zhang et al. in 2019, who showed a temperature resolution of 0.73 °C in hepatic stellate cells within a temperature range from 35 to 43 °C.<sup>53</sup> Also, PAMAM-protected AuNCs demonstrated possible use as nanothermometers.<sup>54</sup> The described AuNC-based temperature probes compare well to already existing fluorescence-based nanothermometers, which present temperature resolutions between 0.1 and 2 °C, with a few exceptions between 0.001 and 0.01 °C.<sup>56</sup> Of these, only a few temperature probes that employ NIR fluorescence to limit interference from autofluorescence of biological samples have been investigated. Green fluorescent protein (GFP) can also serve as a temperature probe and was used to accurately determine the temperature in GFP-transfected HeLa cells with a resolution of 0.4 °C.<sup>57</sup>

The PAMAM-protected AuNCs could also be used for the intracellular sensing of Cr<sub>2</sub>O<sub>7</sub><sup>2-</sup> (dichromate), owing to the fluorescence quenching effects at room temperature in the presence of trace amounts of this ion, with a limit of detection (LOD) of 1.9 μM.<sup>54</sup> AuNCs have been studied quite often for the application of sensitive probes for biosensing. Keratin-Ag-AuNCs<sup>19</sup> have a sensing ability for the heavy metal mercury(II). The LOD was found to be 2.31 nM, showing that these keratin-protected, silver-modified AuNCs are sensitive enough for the detection of mercury in tap water.<sup>19</sup> The sensing of mercury(II) in cellular compartments was also investigated. However, in complex samples the fluorescence quenching effects with increasing mercury concentration were difficult to measure. Yet, it was eventually manageable in fish

samples.<sup>13</sup> GSH-capped AuNCs turned out to be sensitive but not selective to mercury, lead, and copper ions. Besides heavy metals and inorganic ions, the concentrations of small biomolecules and proteins can also be determined by making use of the fluorescence properties of AuNCs.<sup>13</sup> Chicken egg ovalbumin-based AuNCs were employed for biosensing phosphate-containing biomolecules, such as ATP and pyrophosphate.<sup>58</sup> Glucose-oxidase-functionalized AuNCs were able to sense glucose with a lower detection limit of 0.7 μM.<sup>59</sup> Trypsin-stabilized AuNCs, as described by Liu et al. in 2013,<sup>47</sup> were able to sense heparin in human serum samples with a linear range between 0.1 and 4.0 μg/mL and a LOD of 0.05 μg/mL. AuNCs can also be used for the detection and quantification of cancer biomarkers such as neuron-specific enolase,<sup>60</sup> dopamine in the cerebrospinal fluid,<sup>61</sup> interleukin-6,<sup>62</sup> and protein kinase A,<sup>63</sup> among others.<sup>13</sup>

In an additional application, Colombé et al. investigated whether AuNCs could be used for image-guided surgery in mice.<sup>64</sup> In cancers such as head and neck squamous cell carcinoma (HNSCC), tumor resection is difficult due to many complex structures in this area that should not be damaged, such as nerves, tendons, and small muscles. By making use of real-time image-guided surgery, these structures may be preserved while allowing for complete tumor excision with good margins.<sup>64</sup> NIR fluorescence image-guided surgery is a method that has been validated in mice.<sup>65</sup> Because NIR fluorescence provides good optical contrast between healthy and cancer tissue in the case of tumor-targeting fluorescent probes,<sup>65</sup> the probability of efficient tumor resection is improved. Currently, NIR image-guided surgery with the help of fluorophores is under investigation in clinical trials.<sup>66,67</sup> However, the use of AuNCs as an imaging agent is still in the preclinical phase.<sup>64</sup> It was found that NIR image-guided surgery using zwitterionic or pegylated moieties as capping



ligands on AuNCs increases the survival time compared to control animals without image-guidance, as well as the number of mice without any local recurrent tumors due to better detection of tumor residues.<sup>64</sup>

### 3. AUNCS AS A TOOL IN THERAPY

The unique properties of AuNCs are not only useful for bioimaging and diagnostics, but they can also be employed in advanced therapeutic strategies against cancer. AuNCs can assist in radiotherapy or thermal therapy, or facilitate drug delivery.<sup>68–70</sup> Drugs may be encapsulated together with the AuNCs in protein or polymeric scaffolds or can be covalently bound to the capping ligand itself. The therapeutic uses of AuNCs will be discussed in the following section including photothermal and photodynamic therapies, electromagnetic and radiotherapy, and drug delivery. The relevant published studies that employ AuNCs for the purpose of therapy are summarized in Table 3.

**Photothermal and Photodynamic Therapy.** Photothermal therapy (PTT) is a form of phototherapy that is often applied in the treatment of cancer when tumors cannot be removed by surgery.<sup>71,72</sup> In PTT, the destruction of cancer cells is achieved via the induction of hyperthermia, by raising the tumor temperature to 41–47 °C for tens of minutes.<sup>71</sup> By denaturing intracellular proteins and destroying cellular membranes, the tumor cells are killed via apoptosis or necrosis.<sup>73</sup> PTT involves a photothermal agent that is injected in the body either locally or by IV administration. Upon excitation of the photothermal agent, typically by NIR light,<sup>74</sup> photoenergy is converted into thermal energy within the cells that have taken up the photothermal agent.<sup>72</sup> Tumor cells, particularly in the center of the tumor, are more susceptible to heat than healthy cells,<sup>75</sup> improving the selectivity of photothermal therapy. As opposed to bioimaging agents, the ideal photothermal agent has a low fluorescence QY, to obtain an optimal conversion of radiation into heat instead of fluorescence emission.<sup>76</sup>

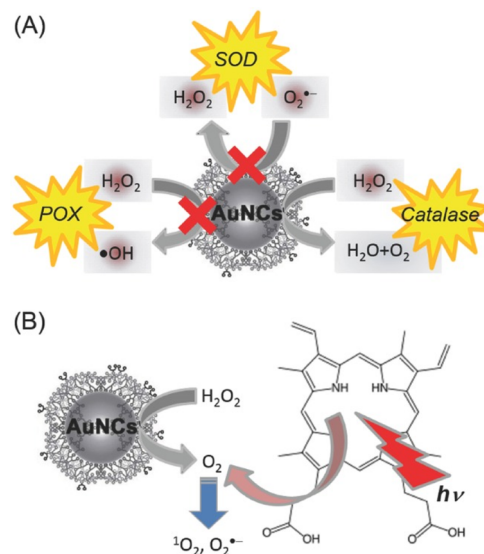
Photodynamic therapy (PDT) is a process that uses a photosensitizer, typically with visible light activation, instead of a photothermal agent. Upon activation, the photosensitizers start generating reactive oxygen species (ROS), thereby eliciting phototoxicity.<sup>77</sup> Advantages that both PTT and PDT have are that they are relatively selective for cancer tissue because of the locally applied light. However, when using either strategy on its own, there are some disadvantages. In PDT there is limited tissue penetration of visible light. Furthermore, singlet oxygen (<sup>1</sup>O<sub>2</sub>), a reactive oxygen species among others that is released upon activation of the photosensitizers, is not always lethal for a whole tumor, owing in part to limited diffusion.<sup>72,78</sup> It is therefore important that the PDT platform is sufficiently small to ensure complete coverage of the tumor. Since the tumor microenvironment is often hypoxic and oxygen is crucial for the effectiveness of PDT, this also creates challenges.<sup>79</sup> In PTT, there is the problem of limited photothermal conversion efficiency<sup>72</sup> and the development of thermotolerance.<sup>71</sup> Because of this, the therapies often need to be combined in order to reduce the risk of relapse or recurring cancer.

Since PTT and PDT work via a different mechanism, combined therapy needs both visible and NIR light activation and different drugs to obtain the desired results.<sup>72</sup> This combination adds complexity and reduces its usability in the clinic. However, AuNCs may provide an opportunity to

combine PTT and PDT in one platform, only requiring a single wavelength for light activation. This was shown by Liu and colleagues in 2019, who reported captopril-stabilized AuNCs that could be used for combined PDT and PTT with near-infrared light activation at a wavelength of 808 nm.<sup>72</sup> They showed a photothermal conversion of 41.1%, laying a strong foundation for promoting the use of AuNCs for PTT. Furthermore, these AuNCs were able to generate enough singlet oxygen for efficient PDT. These results were confirmed *in vivo* by treating cutaneous squamous cell carcinoma tumor-bearing mice with either intratumoral injection of captopril-capped AuNCs combined with light treatment or light treatment alone. It was found that the temperature within the tumor increased by 28.1 ± 6.8 °C in the mice treated with AuNCs compared to 8.4 ± 2.1 °C in mice receiving laser treatment only.<sup>72</sup> Whereas the tumor volumes for all control mice increased, the tumor volumes for the mice that received AuNC treatment decreased significantly. The contributions of PDT and PTT in killing tumor cells *in vivo* was estimated (by use of an ROS scavenger to quench the effect of PDT) to be around 71% and 29%, respectively.<sup>72</sup>

In the literature, there have also been reports on AuNCs designed to reduce hypoxia. An example of this is the reported amine terminated PAMAM dendrimer-encapsulated AuNCs (NH<sub>2</sub>-PAMAM-AuNCs), which have the intrinsic ability to produce O<sub>2</sub> for PDT via catalase-like activity over a broad pH range (see Scheme 3).<sup>80</sup> Because of the extra oxygen present in tumor tissue, the enhanced PDT efficacy was statistically significant. However, the AuNCs themselves were not used for PDT. Instead, an established photosensitizer (protoporphyrin IX) was used. Still, the notion that NH<sub>2</sub>-PAMAM-AuNCs

**Scheme 3. Schematic Illustration of (A) the Enzyme-Like Activities of NH<sub>2</sub>-PAMAM-AuNCs, Which Can Catalyze H<sub>2</sub>O<sub>2</sub> to Produce O<sub>2</sub> via Their Catalase-Like Activity and (B) a Simple Strategy of Conventional PDT Combined with Self-Supplied O<sub>2</sub> via the Catalase-Like Activity of NH<sub>2</sub>-PAMAM-AuNCs, Resulting in an Increase of <sup>1</sup>O<sub>2</sub> and O<sub>2</sub><sup>•-</sup> Generation<sup>a</sup>**



<sup>a</sup>Reproduced with permission from ref 80. Copyright (2017), John Wiley and Sons.

have the ability to alleviate hypoxic conditions could be interesting for future research.<sup>80</sup>

**Radiation and Electromagnetic Therapy.** Nowadays, one of the leading therapeutic options for treating cancer is radiotherapy.<sup>81,82</sup> Radiotherapy kills tumor cells via treatment with high energy radiation, typically megavolt X-ray or gamma ray radiation with a dose between 3 and 6 Gy.<sup>81,83</sup> While it is generally very effective, one of the main setbacks of this treatment option is that it can also cause serious damage to the healthy tissues surrounding the tumor site.<sup>81</sup> When using a radiosensitizer, the efficacy of a radiation dose is increased.<sup>81</sup> This way, a lower radiation dose can be used for the therapy, one that is relatively safe to healthy cells that have not taken up the radiosensitizer. Radiosensitizers also enhance the outcome of radiation therapy, even when tumor cells are radioresistant (e.g., hypoxic).<sup>84</sup> When a radiosensitizer is irradiated with X-rays, secondary effects are generated, for example, scattered photons, electrons, electron–positron pairs, or fluorescence. These secondary effects can then aid in destroying cells.<sup>84</sup> Gold is an especially good radiosensitizer, considering its large atomic number and its therefore high absorbance of radiation, which leads to an enhancement of radiotherapy of up to a 100 times compared to tissue without radiosensitizer.<sup>84</sup> While larger gold nanoparticles have already been studied for their potential in radiation therapy, the disadvantage of limited *in vivo* applicability because of unsatisfying biodistribution and clearance<sup>85</sup> has provided incentive for the smaller AuNCs to be investigated for this application as well.

GSH-capped and BSA-capped AuNCs were tested for enhancement of radiotherapy, by Zhang et al. in 2014.<sup>83</sup> *In vitro* studies demonstrated that the GSH- and BSA-AuNCs enhanced the radiosensitivity by 30% and 21%, respectively, relative to radiation alone. This difference may be due to improved cell uptake of GSH-AuNCs because of their smaller size or zwitterionic surface chemistry. *In vivo*, the GSH-AuNCs with radiation showed a statistically significant decrease in tumor growth, where after 20 days, the tumor volume was 35% smaller compared to the tumor after radiation alone. The BSA-AuNCs, however, had no significant reduction in tumor growth after treatment compared to their control, showing a difference with radiation alone of around 10%.<sup>83</sup>

Gahremani et al. investigated BSA-AuNCs for the purpose of megavoltage radiation therapy of breast cancer cells.<sup>86</sup> Using an AS1411 aptamer moiety conjugated to the BSA-AuNCs as a targeting agent for nucleolin, they were able to efficiently target these cancer cells. *In vitro* it was found that the combination of the Aptamer-BSA-AuNCs with megavoltage radiation therapy (between 6 and 25 MV)<sup>84</sup> leads to efficient cancer cell death, enhanced by the AuNCs with a factor of 2.7 compared to controls.<sup>86</sup> Besides that, Cifuentes-Rius et al. found that BSA-AuNCs can also be applied in electromagnetic radiation therapy.<sup>87</sup> Upon 8 min light activation with 15 W microwaves (1 GHz electromagnetic fields), cell viability decreased in six types of mammalian cell lines. At a gold concentration of 50  $\mu\text{g/mL}$ , approximately 50% of the B-lymphocytes, 68% of prostate cancer cells, and 28% of neuroblastoma cells died via induction of apoptosis and necrosis.<sup>87</sup>

**AuNCs as a Platform for Drug Delivery.** AuNCs have been reported to act as a tool for drug delivery itself, primarily without light activation. For example, the natural flavonoid kaempferol was conjugated to BSA-protected AuNCs via physical interactions and tested for its anticancer properties in lung cancer cells.<sup>88</sup> Flavonoids are well-known for their

antioxidant activity and can possibly be used for the treatment of cancer,<sup>88–91</sup> microbial infection, and angiogenesis, among others.<sup>89</sup> While showing little to no cytotoxicity in healthy human kidney cells, kaempferol-BSA-AuNCs were able to kill over 50% of the cancer cells at a concentration of 25  $\mu\text{g/mL}$  *in vitro*. Additionally, the kaempferol-BSA-AuNCs were shown to slow down the migration rate of HeLa cells. Although the purpose of the AuNCs within the drug delivery system was to provide imaging possibilities ( $\lambda_{\text{ex}}/\lambda_{\text{em}} = 550/650 \text{ nm}$ ), no cell imaging experiments have been reported.<sup>88</sup>

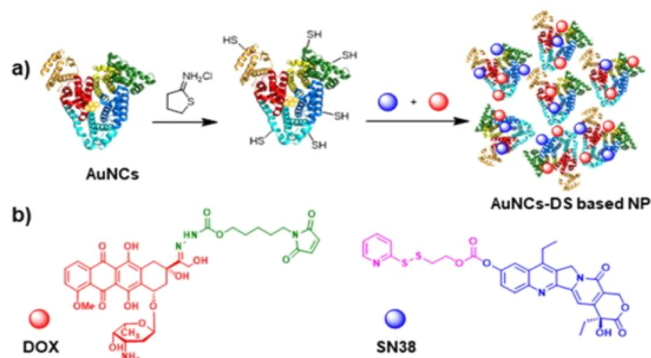
In a similar manner, Lakshmi et al. synthesized a flavonoid based drug delivery system, using quercetin as drug conjugate.<sup>91</sup> The quercetin was bound to BSA-AuNCs via Au–OH interactions and showed good cellular uptake. The intention of the AuNCs was to use them for their fluorescent bioimaging properties ( $\lambda_{\text{ex}}/\lambda_{\text{em}} = 360/568 \text{ nm}$ ), but since these results were not reported on cellular experiments, the quercetin-BSA-AuNCs are not considered theranostic here. They did show high cytotoxicity in lung cancer cells, whereas minimal cell death occurred in healthy fibroblasts.<sup>91</sup>

There has also been research for a drug carrier using AuNCs that focuses on controlled drug release. Latorre et al. published an article in 2019 where BSA-AuNCs were investigated as nanocarriers for combined chemotherapy against cancer, targeting mainly cancer stem cells.<sup>92</sup> To this end, they functionalized the BSA-AuNCs with both doxorubicin (DOX) and a camptothecin analogue SN38 to inhibit topoisomerase II and I in target cells. Herein, the AuNCs serve only as a structural scaffold. Although the results in clinical trials for the combination of free DOX and SN38 have not been satisfactory, it has previously been shown to be one of the most synergistic combinations of chemotherapy when injected as a polymer–drug conjugate.<sup>93</sup> Thiols were introduced to the BSA by reacting the BSA-AuNCs with 2-iminothiolane. SN38 was then coupled to BSA with a redox-sensitive linker that is cleaved in a reducing environment, which contains, for example, a relatively high concentration of glutathione. DOX was modified with a pH-sensitive linker that breaks in a slightly acidic environment, as is the case in endosomes and lysosomes. The disulfide bond and maleimide in the linkers enabled conjugation to the thiols of BSA. A schematic overview of the synthesis and the modified chemotherapeutics is depicted in Scheme 4.<sup>92</sup> *In vitro* toxicity studies in MCF7, MDA-MB-231, and Panc-1 cells showed that the BSA-AuNCs with both chemotherapeutics exhibited enhanced cytotoxicity compared to BSA-AuNCs with only one of the drugs. These bifunctionalized AuNCs were shown to induce highly efficient DNA damage, allowing their effective use against cancer stem cells by significantly reducing the size and number of mammospheres at concentrations as low as 0.08  $\mu\text{M}$ .<sup>92</sup>

AuNCs have not only been investigated as a drug carrier *in vitro* and *in vivo*. El-Mageed et al. found *in silico* that AuNCs have the ability to act as a drug delivery system for D-penicillamine in cancer treatment.<sup>94</sup> This research focused mostly on modeling the potential interactions and binding energies between D-penicillamine and gold. It was found that the drug would be coupled to the gold core mainly via physical interactions. Examples of these are the Au–O/S/N bonds, hydrogen bonds, and electrostatic bonds.<sup>94</sup>

Recently, Hebels et al. reported a first-in-class platform employing AuNCs for light induced tumor cell killing.<sup>11</sup> The AuNCs were formed into a stabilized core-cross-linked micelle

**Scheme 4.** (A) Schematic Overview of Synthesis of DOX and Camptothecin SN38 Functionalized BSA-AuNCs (Depicted as Coils with Small Yellow Circles in the Center). (B) DOX (red) Modified with pH-Sensitive Linker (Green) and SN38 (Blue) Modified with a Redox-Sensitive Linker (Pink)<sup>a</sup>



<sup>a</sup>Reproduced with permission from ref 92. Copyright (2019), Multidisciplinary Digital Publishing Institute.

system based on PEG and thermosensitive poly(*N*-isopropylacrylamide) (PNIPAM). These micelles contained free thiols from cysteine moieties incorporated into the system. A QY of 3% was reported ( $\lambda_{\text{ex}}/\lambda_{\text{em}} = 550/720 \text{ nm}$ ). Thiol-containing DOX (DOX-SH) was obtained by thiol modification of DOX with 2-iminothiolane and then covalently linked into the AuNCs during their formation. This DOX-SH-AuNC micelle formulation was shown to be toxic to MDA-MB-231 breast cancer cells upon light activation with a 650 nm laser in a highly localized fashion, highlighting the potential use of AuNCs as a tool in laser-guided drug release therapies.<sup>11</sup>

#### 4. AUNCS EMPLOYED IN THERANOSTIC PLATFORMS

According to Kelkar et al., the ultimate goal of the theranostic field is to design a single agent that provides the ability to image and monitor diseased tissue, while also showing sufficient drug delivery and treatment efficacy.<sup>14</sup> In this section, a review is given on the current advances in theranostic approaches employing AuNCs. Herein, a division is made between three types of theranostic platforms, depending on the function of the AuNCs within the whole complex. The AuNCs can be used solely for imaging, namely, in cellular imaging experiments, be only employed for their ability to aid in therapeutic approaches, or have a function in both imaging and therapy. Table 3 summarizes the articles that are mentioned in the following section, to provide a comprehensive overview.

**Theranostic Systems Employing AuNCs as a Tool for Imaging.** In 2012, an article was published by Chen et al., who synthesized a drug delivery system by combining BSA-capped AuNCs, poly(*L*-lactide) (PLA) and a folic acid-conjugated sulfated polysaccharide (GPPS-FA).<sup>95</sup> The BSA-AuNCs formed the core of the particles, PLA the inner shell, and GPPS-FA the outer shell with FA as targeting moieties. Camptothecin was used as a hydrophobic anticancer drug that was encapsulated in the PLA inner shell of the nanocarrier. The drug-release profile showed a rapid release in the first hour due to adsorption or weak interactions in the hydrophilic shell, followed by sustained release up to 15 h from the hydrophobic fraction. Interestingly, the empty nanocarriers already exhibited

a mild cytotoxicity in HeLa cells, which was significantly enhanced when the nanocarriers were loaded with camptothecin by encapsulation. Imaging was performed *in vitro* by confocal scanning microscopy on HeLa cells ( $\lambda_{\text{ex}} = 496 \text{ nm}$ ).<sup>95</sup>

A good example of a theranostic approach in drug delivery and cancer bioimaging, where AuNCs are solely used for their fluorescent properties, was developed by Muthu et al. in 2015.<sup>96</sup> They designed a vitamin E tocopheryl polyethylene glycol 1000 succinate (TPGS) micelle conjugated with transferrin for transferrin-targeted codelivery of the drug docetaxel and fluorescent AuNCs. Docetaxel and the AuNCs were encapsulated in the lipophilic core of the micelle. The system exhibited cytotoxic properties in transferrin receptor overexpressing breast cancer cells, and the micelles emitted fluorescence ( $\lambda_{\text{ex}}/\lambda_{\text{em}} = 365/620 \text{ nm}$ ) *in vitro*. The biodistribution proved to be satisfactory with a good clearance, where the transferrin-targeted micelles reached an IC<sub>50</sub> value 72-fold lower than that of the FDA-approved docetaxel formulation.<sup>96</sup>

Croissant et al. managed to develop a nanocarrier system that encapsulated both gemcitabine and DOX in a mesoporous silica nanoparticle containing BSA-AuNCs for the treatment of ovarian and breast cancers.<sup>97</sup> In this theranostic system, the AuNCs were not involved in the encapsulation of the drugs. Gemcitabine and DOX were both immobilized with an acid-sensitive linker and released with a pH trigger that resulted in almost complete killing of cancer cells. The biodistribution of the entire system was investigated by imaging ( $\lambda_{\text{em}} = 600 \text{ nm}$ ) *in vivo*, showing good tumor targeting efficiency.<sup>97</sup>

**Theranostic Systems Employing AuNCs as a Tool for Therapy.** An approach to a dual-targeting theranostic platform was looked into by Chen et al. in 2016.<sup>98</sup> *L*-Histidine-capped AuNCs were coupled to cyclic RGD for extracellular targeting, and to the aptamer AS1411 for nuclear targeting. DOX was then immobilized onto the nanocarrier by forming a covalent bond between the primary amine on DOX and the activated carbonyl group of histidine. This formed a drug-delivery system with a high tumor cell affinity. However, a distinct drug release profile has not been reported. Still, cancer cell inhibition occurred *in vitro* as well as *in vivo*. Using the quadrupolar anthracene-based near-infrared dye MPA, the complex showed potential toward bioimaging applications.<sup>98</sup>

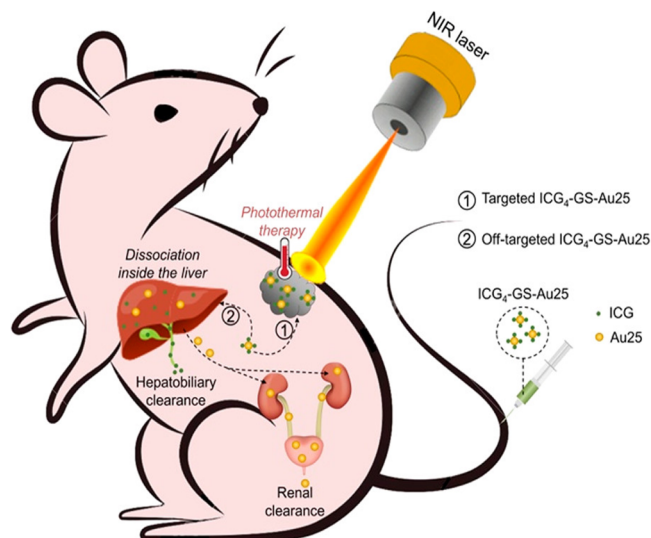
AuNCs can also be applied in formulations for the delivery of biological drugs. Lei et al. reported the synthesis of GSH-oligoarginine-capped AuNCs as a nanocarrier for delivery of nerve growth factor (NGF) small interfering RNA (siRNA) in pancreatic cancer.<sup>99</sup> The use of AuNCs to assist in the delivery of siRNA was shown to be beneficial, considering that the gold increased the stability of siRNA in serum, as well as the circulation time, cellular uptake, and tumor accumulation *in vivo*. With the help of the Cy5 NIR dye, the uptake in cells was visualized by fluorescence. In an *in vivo* subcutaneous model, the average tumor growth was reduced by 52% compared to saline control. In the orthotopic pancreatic cancer model in Balb/c nude mice, it was shown that the designed formulation decreased tumor sizes compared to saline controls while also showing a low expression level for NGF mRNA and NGF protein. The aim to target tumor–neuron interaction by silencing the NGF gene in pancreatic cancer to inhibit progression was therefore fulfilled.<sup>99</sup>

Jiang et al. demonstrated that GSH-AuNCs coupled to the fluorescent dye indocyanine green (ICG) via amide coupling could enable a switchable fluorescence and enhance the



photothermal efficacy of free ICG (see Scheme 5).<sup>100</sup> When coupled to the GSH-AuNCs, the fluorescence of the ICG was

**Scheme 5. Schematic Representation of ICG-GSH-AuNC Mediated Photothermal Cancer Therapy and Their *In Vivo* Clearance Pathways after Dissociation in the Liver<sup>a</sup>**



<sup>a</sup>Reproduced from ref 100. Copyright (2020), American Chemical Society.

almost completely quenched. However, it was instantaneously recovered once ICG was released ( $\lambda_{\text{ex}}/\lambda_{\text{em}}$  ICG = 760/825 nm). The gold itself does not show any fluorescence at this excitation wavelength. It was found that the photochemical stability of ICG increased due to conjugation with the GSH-AuNCs. During a 15 min light activation *in vitro*, a rapid increase in temperature of approximately 20 °C was seen, with minimal decay. By contrast, free ICG and free GSH-AuNCs only exhibited a slight temperature increase, of approximately 10 and 5 °C, respectively. ICG-GSH-AuNCs also showed reduced inherent cytotoxicity compared to free ICG, suggesting that the efficient tumor killing is primarily achieved through PTT. *In vivo*, mice were irradiated with the laser for 8 min at a power density of 0.8 W/cm<sup>2</sup>, showing similar results to *in vitro* studies. After PTT with ICG-GSH-AuNCs, the breast cancer tumors disappeared within 2 weeks, whereas PTT with free ICG or PBS displayed no therapeutic efficacy. This might partially be because the AuNCs prolong the blood circulation and enhance tumor targeting, as well as increase the photothermal performance compared to free ICG.<sup>100</sup>

**Theranostic Systems Employing AuNCs for Imaging and Therapy.** AuNCs have often been described for the simultaneous imaging and delivery of chemotherapeutic drugs. An example is described in the study of Zhou et al.<sup>101</sup> In this work, cisplatin is delivered as a prodrug conjugated to folic acid functionalized BSA-AuNCs to metastasised breast cancer. The drug release for this chemotherapy was based on a redox sensitive linker that coupled the cisplatin to the AuNCs. The AuNCs were then tested for their fluorescence ( $\lambda_{\text{ex}}/\lambda_{\text{em}}$  = 415/670 nm) and biodistribution *in vivo*. Here, the AuNCs showed good tumor targeting efficiency with inhibition of growth and lung metastasis of 4T1 tumors, while avoiding accumulation in healthy organs.<sup>101</sup>

Khandelia et al. also investigated BSA-capped AuNCs, but for the delivery of DOX with concurrent single-photon or two-photon imaging of cancer cells.<sup>102</sup> They determined that the emission by two-photon fluorescence falls within the NIR range ( $\lambda_{\text{ex}}/\lambda_{\text{em}}$  = 505/655 nm), thereby showing promise for *in vivo* imaging. They also tested the cytotoxicity of the empty BSA-AuNCs and the release of DOX to human cervical cancer cells *in vitro*. It was found that the BSA-AuNCs had no inherent cytotoxicity. When DOX was implemented, an IC<sub>50</sub> of 6.3 µg/mL of DOX was determined, which is less toxic than free DOX (IC<sub>50</sub> = 0.82 µg/mL). This could possibly be explained by incomplete release of DOX over the 36 h incubation time.<sup>102</sup>

By inhibiting the EGFR, VEGFR, and AKT signaling pathways using the dual drugs vandetanib and epigallocatechin gallate (EGCG), Kumar et al. showed a way to circumvent tamoxifen-resistance in breast cancer cells.<sup>103</sup> They designed a mesoporous silica drug delivery system that encapsulates EGCG. The silica particles are then modified to present thiols at their surface, followed by covalent bonding of AuNCs via gold–thiol interactions. Vandetanib was then coupled to the AuNCs to form the complete nanocarrier. Using the fluorescence of the AuNCs ( $\lambda_{\text{ex}}/\lambda_{\text{em}}$  = 530/670 nm), the nanocarrier could be localized intracellularly. Tumour growth was delayed *in vivo* by the inhibition of EGFR, VEGFR, and AKT. Considering that these proteins are overexpressed in tamoxifen-resistant cancer cells, inhibiting them may sensitize the tumor cells to tamoxifen chemotherapy.<sup>103</sup>

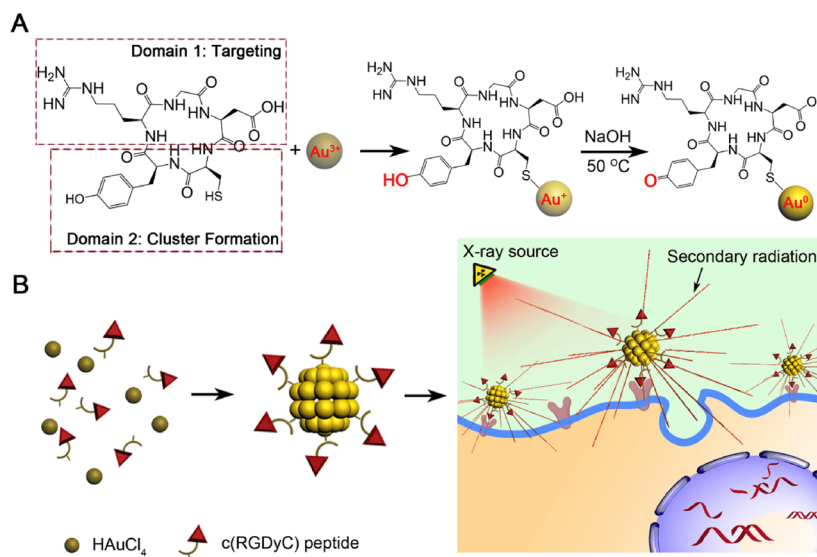
The flavonoid curcumin<sup>89,90</sup> has been investigated as a drug-conjugate in theranostic systems as well. Curcumin-capped AuNCs were brightly fluorescent ( $\lambda_{\text{ex}}/\lambda_{\text{em}}$  = 550/650 nm). Furthermore, curcumin-AuNCs showed almost no toxicity in mortal cell lines (~100% cell survival) compared to a high lethality in human cervical cancer cells (~15% cell survival) at a concentration of 100 µg/mL. The drug delivery system also caused a reduction of the HeLa cell migration rate.<sup>89</sup> In another study on curcumin-BSA-AuNCs,<sup>90</sup> the nanocarriers exhibited a higher inhibition efficiency in neuroblastoma tumor cell growth than free curcumin or BSA-AuNCs alone, with an IC<sub>50</sub> value of 14.3 nM. In fact, there appeared to be a synergistic induction of cellular apoptosis for this particular nanocarrier system.<sup>90</sup>

Wang et al. found that when the phosphatase and tensin homologue (PTEN) tumor suppressor gene is conjugated to AuNCs, the complex can be used to inhibit liver tumor growth as well as fluorescent imaging.<sup>104</sup> Using the low pH and high concentration of reductive substances (e.g., GSH and NADP<sup>+</sup>) in the tumor microenvironment, PTEN-AuNCs were synthesized *in situ* by injecting the AuNC precursor and PTEN DNA. It was subsequently found that the PTEN-AuNC complexes can inhibit or even prevent liver tumor proliferation, invasion, and metastasis *in vitro*. Additionally, cancer growth was inhibited significantly in mice, and the imaging possibilities of the complex were also shown.<sup>104</sup>

Chen et al. investigated HSA and catalase comodified alkyl thiolated AuNCs (AuNC-HSA/CAT) in photodynamic therapy combined with fluorescent imaging ( $\lambda_{\text{ex}}/\lambda_{\text{em}}$  = 365/600–650 nm).<sup>79</sup> Using the NIR-II region for light activation with a wavelength of 1064 nm for 20 min, they showed that PDT utilizing AuNCs is indeed possible at this long wavelength. Because the CAT moiety is also attached to the AuNCs, the problem of hypoxia in the tumors was alleviated. This was illustrated by a significant tumor volume reduction



**Scheme 6. Schematic Illustration of RGD Peptide-Modified AuNC Formation and Application for Enhanced Radiotherapy.** (A) The Cysteine and Tyrosine Residues Capture  $\text{Au}^{3+}$  Ions and Reduce Them to  $\text{Au}^0$  under Alkaline Conditions, Respectively. (B) RGD Peptide-Modified AuNCs Accumulate in  $\alpha_v\beta_3$  Integrin-Positive Cancer Cells and Interact with Incident Radiation Intensively, Generating Secondary Radiation, and Leading to Radiation Enhancement Effect<sup>44</sup>



<sup>44</sup>Reproduced with permission from ref 81. Copyright (2017), Elsevier.

when performing PDT with the AuNC-HSA/CAT, compared to a moderate inhibition of tumor growth for the AuNC-HSA. Treatment with the laser or AuNC-HSA/CAT alone had no effect on tumor volume.<sup>79</sup>

Radiation therapy was also explored as a modality in theranostic AuNCs by Liang et al. They proposed to use RGD peptide-modified AuNCs as tumor-targeting radiotherapy enhancers (see Scheme 6).<sup>81</sup> With this particular targeting moiety, the  $\alpha_v\beta_3$  integrin-positive cancer cells can be stained and then killed by radiotherapy with a higher efficacy compared to radiation alone. For the mice treated with the RGD peptide-modified AuNCs and radiotherapy, the tumor volume only increased by 30% over a period of 14 days, compared to an increase of over 130% for radiation alone. The RGD peptide-modified AuNCs were shown to have inherent fluorescent properties ( $\lambda_{\text{ex}}/\lambda_{\text{em}} = 488/660$  nm), as well as CT imaging capabilities.<sup>81</sup>

In 2019, Luo et al. described cysteine-tyrosine-prostate specific membrane antigen-targeted AuNCs (CY-PSMA-AuNCs) as radiosensitizers for therapy of prostate cancer.<sup>84</sup> Besides radiosensitization, the CY-PSMA-AuNCs also had *in vitro* fluorescent ( $\lambda_{\text{ex}}/\lambda_{\text{em}} = 490/700$  nm) and *in vivo* CT properties. Fast elimination of the CY-PSMA-AuNCs from the mice via renal clearance was observed during the biodistribution studies. *In vivo* testing showed that the tumor growth was inhibited much better in mice bearing PSMA over-expressing tumors as compared to negative tumors after IV injection. In both cases, 18 days after being given a radiation dose of 6 Gy, the tumor size increased by only 94% and 311%, respectively. Compared to the control mice with PBS injections plus radiation, who exhibited a tumor growth of up to 430%, these results show that the AuNCs indeed act as radiosensitizers and by functionalization with PSMA show potential for active targeting applications.<sup>84</sup>

Al Zaki et al. synthesized polymeric micelles loaded with AuNCs for the application of CT-guided radiation therapy, where the AuNCs act as radiosensitizers.<sup>40</sup> The micelles,

consisting of an amphiphilic diblock polymer poly(ethylene glycol)-*b*-poly( $\epsilon$ -caprolactone), contained tightly packed 1.9-nm-sized AuNCs (GPMs). It was determined *in vivo* that following IV injection, the GPMs served as imaging contrast agents for CT imaging, which were used for better visualization of the tumor boundaries. The GPMs exhibited a radiosensitization enhancement ratio of approximately 1.2 *in vitro*, while a statistically significant improved survival rate was observed in tumor-bearing mice treated with GPMs compared to radiotherapy without GPMs.<sup>40</sup>

Some theranostic platforms have been developed to incorporate imaging and multiple types of therapy together. An example of this is the AuNC containing vehicle designed by Yang et al. in 2019.<sup>105</sup> GSH-capped AuNCs conjugated to graphene oxide functionalized with hyaluronic acid as targeting agent were synthesized for fluorescent image-guided synergetic delivery of 5-fluorouracil and phototherapy. Because of the inhibition of the fluorescence of the AuNCs in the presence of graphene oxide, controlled fluorescence turn-on imaging can be realized. Upon cleavage of the glycosidic linkages by hyaluronidase, the HA-GSH-AuNCs were released from the graphene oxide, leading to restoration of the fluorescence ( $\lambda_{\text{ex}}/\lambda_{\text{em}} = 580/675$  nm). Subsequently, under light activation at 638 nm, photodynamic therapy could occur. Besides that, the light activation caused the loaded 5-fluorouracil to be released quickly and the graphene oxide to exhibit its photothermal properties. This leads to an enzyme and laser-controlled fluorescence, along with chemotherapeutic, photothermal, and photodynamic functionalities. *In vitro* cytotoxicity studies showed the efficacy of the triple therapy where 84.3% of the lung cancer cells died, which was significantly enhanced compared to the chemotherapy or phototherapy alone.<sup>105</sup>

Li et al. designed the aforementioned (Table 1) keratin-templated AuNCs functionalized with silver and gadolinium ions.<sup>23</sup> They showed an enhanced fluorescence intensity, biocompatibility, and colloid stability, and were able to provide *in vivo* MRI as well as NIR fluorescence imaging ( $\lambda_{\text{ex}}/\lambda_{\text{em}} =$

525/710 nm). Subsequently, under light activation at 638 nm, photodynamic therapy could occur. Besides that, by employing a redox-sensitive linker, DOX could be selectively released in cancer cells where the concentration of glutathione is high, at both neutral and low pH. In breast cancer bearing mice, the formulation achieved a significant reduction of tumor growth.<sup>23</sup>

Besides acting as sensitizers in radiotherapy, as agents in phototherapy, and drug delivery applications, AuNCs themselves can also show therapeutic efficacy. Wang et al. developed a therapy involving *in situ* biosynthesized AuNCs that could effectively slow down tumor progress by inhibiting the activity of the PI3K-AKT pathway.<sup>106</sup> It was found that 24 h after a tail vein injection with HAuCl<sub>4</sub>, 2.5-nm-sized AuNCs had formed in the liver tumor, while also showing that the AuNCs were preferentially formed at that site by measuring their intrinsic fluorescence. After 38 days, the tumors of the mice treated with the AuNCs exhibited reduced growth compared to mice treated with PBS injections. By performing RNA-sequence analysis it was determined that the expression of proteins targeted by the PI3K-AKT signaling pathway had decreased. This was further confirmed by real-time PCR and Western blots *in vitro*. Based on these results, the authors speculated that the inhibition of the PI3K-AKT pathway was the main cause of the observed reduction in tumor growth upon treatment with *in situ* biosynthesized AuNCs.<sup>106</sup>

## 5. AUNCS FOR OTHER THERAPEUTIC APPLICATIONS

AuNCs have not only been investigated for their unique properties in cancer bioimaging, therapy, and theranostic systems, but have also shown promise in other areas of biomedical research such as vaccine development and treatment or prevention of bacterial infection. Recent interest regarding the applicability of AuNCs in central nervous system (CNS) disorders has emerged as well. To provide an overview, the articles mentioned in the following section have also been summarized in Table 3.

**AuNCs in Vaccine Development.** Several research groups have investigated AuNCs for their immunological properties as well as their potential toward simultaneous fluorescence imaging.<sup>107–109</sup> Fernández et al. studied the immunological properties of AuNCs in human dendritic cells (DCs), as well as their cellular uptake.<sup>107</sup> Using the fluorescence intensity of the AuNCs, they found that the zwitterionic AuNCs were readily taken up by DCs, which subsequently triggered DC maturation. This was achieved to a lesser extent with PEGylated AuNCs and larger gold nanoparticles. Immunological analysis revealed that the zwitterionic AuNCs cause T helper 1 and T regulatory cell responses, while not leading to proliferation of natural killer cells and cytotoxic T cells. These results encourage the further investigation of AuNCs in vaccines.<sup>107</sup>

In 2014, Tao et al. had already looked into AuNCs as vaccines using dual-delivery of an antigen and an adjuvant, while the AuNCs simultaneously acted as an imaging agent.<sup>108</sup> To this end, they conjugated the adjuvant cytosine-phosphate-guanine (CpG) oligodeoxynucleotides (ODNs) to the antigen ovalbumin and used this as a template for the synthesis of the AuNCs. Based on the secretion of immunostimulatory cytokines TNF- $\alpha$  and IL-6, it was determined that the AuNC containing system induced the maturation of APCs. It was also found that the concurrent delivery of the CpG ODNs and of ovalbumin enhanced cellular immunity. Besides that,

the conjugation of CpG ODN and ovalbumin to the gold caused an increased stability and enhanced cellular uptake, further increasing immunostimulatory activities. The notion that the AuNCs could therefore be used as vaccine vehicle was then further confirmed in mice, which developed an enhanced antiovalbumin IgG response.

Wang et al. aimed to develop a vaccine against hepatitis E, by preparing AuNCs *in situ* within the monomers of the hepatitis E vaccine (HEVA).<sup>110</sup> The presence of AuNCs caused a facile synthesis of HEVA aggregates (HEVA/Au), which possess high potency in provoking antibody responses compared to the single monomers. The inherent blue fluorescence of the HEVA/Au solution allowed for tracking of the vaccine aggregates in cells and *in vivo* ( $\lambda_{\text{ex}}/\lambda_{\text{em}} = 365/410$  nm, QY = 6%). Cell uptake experiments showed that the HEVA/Au was easily taken up by the liver and immune cells, where it was mainly present in the cytosol and lysosomal compartments. *In vivo* biodistribution studies showed accumulation of HEVA/Au in the liver, heart, kidney, lymph nodes, and spleen. Whereas HEVA was toxic at concentrations above 0.1 mg/mL, HEVA/Au showed no cytotoxicity at a concentration of 1 mg/mL, displaying its improved safety profile. Furthermore, the antibody immune response was enhanced by the HEVA/Au, by influencing the Th1/Th2 immune response *in vivo*.<sup>110</sup>

**AuNCs in the Prevention and Treatment of Bacterial Infection.** Phototherapy is not only useful in treating cancer but can also be applied for dispersing biofilms. In 2020, Xie et al. published a study that investigated the potential of DNase-functionalized AuNCs in eradicating bacteria that are shielded by biofilms.<sup>111</sup> They reported that DNase can assist in enzymolysis, thereby breaking down the extracellular polymeric substance matrix, which subsequently exposes the bacteria to the AuNCs. PDT and PTT were then induced by 808 nm light activation. With a photothermal conversion of 6.6% and abundant ROS generation, the combination led to killing of approximately 90% of the biofilm-shielded bacteria. No additional photosensitizer was employed and the <sup>1</sup>O<sub>2</sub> species detected originate from the DNase-functionalized AuNCs themselves.<sup>111</sup>

AuNCs have also been investigated as a bactericidal agent itself. Zheng et al. developed 6-mercaptohexanoic acid-protected AuNCs that could kill both Gram-positive (*S. aureus*, *S. epidermidis*, *Bacillus subtilis*) and Gram-negative (*E. coli*, *Pseudomonas aeruginosa*) bacteria owing to their small size when compared to gold nanoparticles.<sup>112</sup> At a concentration of 0.1 mM on the basis of Au atoms, the AuNCs killed more than 90% bacteria within 2 h of incubation. It was found that the AuNCs exhibit an IC<sub>50</sub> against *S. aureus* comparable with widely used antibiotics such as ampicillin and penicillin.<sup>112</sup>

Jiang et al. also prepared quaternary ammonium-glutathione-capped AuNCs (QA-GSH-AuNCs) for the treatment of multidrug-resistant (MDR) Gram-positive bacteria, such as methicillin-resistant *S. aureus* (MRSA) and vancomycin-resistant *Enterococci* (VRE).<sup>113</sup> The QA-GSH-AuNCs exhibited bright fluorescence that could be used for bacterial cell counting ( $\lambda_{\text{ex}}/\lambda_{\text{em}} = 362/592$  nm). Because of the positive charge of the capping ligand, the QA-GSH-AuNCs were able to penetrate the bacterial cell wall and damage it. This was followed by ROS formation and disruption of intracellular metabolic pathways, thereby killing the bacteria. By comparing the QA-GSH-AuNCs to commonly used antibiotics, it was found that the time-kill kinetics are similar, and that the dose-

dependent inhibition of *S. aureus* growth was like that of vancomycin. Interestingly, it was shown that the QA-GSH-AuNCs had a broader antibacterial spectrum than any of the tested established antibiotics (ampicillin, oxacillin, linezolid, and vancomycin), including for VRE and MRSA, without inducing drug resistance at sub-inhibitory levels. *In vivo*, the toxicity to healthy cells and elimination half-life ( $7.5 \pm 2.1$  h) was satisfactory. The QA-GSH-AuNCs were able to prevent death of mice infected with MRSA for 16 days at a concentration of 40 mg/kg, which was similar to the effective dose of vancomycin.<sup>113</sup>

As a follow-up study, Xie et al. aimed to use the QA-GSH-AuNCs for the prevention of oral biofilm formation, also called plaque, to reduce bacterial infection of teeth caused by Invisalign aligners.<sup>114</sup> This was done by allowing the QA-GSH-AuNCs to adsorb onto the aligners to make an antibacterial coating against *S. mutans*. The QA-GSH-AuNCs have a minimal inhibitory concentration of 4  $\mu\text{g}/\text{mL}$  *in vitro*, killing the bacteria via destruction of the membrane integrity. The QA-GSH-AuNCs showed negligible toxicity and inflammation in mice but were highly efficient in preventing the attachment and biofilm development of *S. mutans*, *S. aureus*, *S. epidermidis*, and their MDR counterparts. It was found that the *S. mutans* biofilms had 85% less biomass and 95% less cell viability on QA-GSH-AuNCs-coated aligners. The antibacterial activity of the coated aligners was shown to remain present for several cycles of use and after storage for three months. This approach could be extended to many other medical devices to reduce bacterial-induced oral diseases.<sup>114</sup>

Very recently, a modification of Auranofin, an FDA-approved gold(I)-complex with tetraacetylated thioglucose ( $\text{Ac}_4\text{GlcSH}$ ) and triethylphosphine ( $\text{PET}_3$ ) ligands employed as anti-inflammatory aid in rheumatoid arthritis, was reported for use as a nanoantibiotic.<sup>115</sup> Here, AuNCs (instead of gold(I)) were functionalized with mixed phosphine and glycolyl thiol ligands by ligand exchange of  $\text{PPh}_3$ -capped AuNCs. This resulted in improved activity against MDR *P. aeruginosa* (up to 4-fold) while reducing cytotoxicity to human A549 cells (up to 24-fold) when compared to Auranofin, further highlighting the potential of AuNCs in antimicrobial applications.<sup>115</sup>

**AuNCs in Central Nervous System Disorders.** Another application of AuNCs that has gained recent interest, is their ability to cross the blood-brain-barrier (BBB) owing to their small size.<sup>116</sup> Because of this, Xiao et al. explored the potential of dihydrolipoic acid-capped AuNCs as probes for therapy in central nervous system (CNS) disorders, such as traumatic brain injury, stroke, Parkinson's Disease (PD), and Alzheimer's disease,<sup>116</sup> by detecting neuroinflammation. They found that these AuNCs could effectively reduce proinflammatory processes in microglial BV2 cells *in vitro*, indicating that these dihydrolipoic acid-capped AuNCs have potential to become a therapeutic agent in CNS disorders.<sup>116</sup>

Another example of AuNCs acting as a therapeutic agent in CNS disorders was reported by Gao et al. in 2019.<sup>117</sup> Based on their results, they suspect that *N*-isobutyryl-L-cysteine (L-NIBC) protected AuNCs can serve as a novel form of therapeutics for the treatment of PD. They found that *in vitro* the L-NIBC-AuNCs prevent the aggregation and fibril formation of  $\alpha$ -Synuclein, while having a neuroprotective effect and improving behavioral disorders in a PD mouse model *in vivo* at a dose of 20 mg/kg.<sup>117</sup>

## 6. DISCUSSION

In the past two decades, the NIR fluorescence of AuNCs, its origin, and how to tune it have been thoroughly studied. Design strategies using proteins, peptides, or other biological molecules as structural scaffolds for the synthesis of AuNCs were developed to preserve the AuNCs' attractive photoluminescent properties while increasing the biocompatibility. This paved the way for the use of AuNCs in NIR fluorescent bioimaging. AuNCs were also investigated for therapeutic applications, involving drug delivery, phototherapy, and radiotherapy, among others. In particular, a lot of research focused on combining imaging and therapy in a single platform. Although many different definitions exist of what a theranostic platform is, in this review AuNC-containing platforms are considered theranostic when the imaging and therapeutic properties have been tested in cellular experiments or *in vivo*.

Looking at the extensive research done on the topic of AuNCs as theranostic tools, particularly in cancer, numerous approaches have been investigated so far; yet, there has been no report of AuNCs being investigated in clinical trials. There is a chance that this is simply because AuNCs are a relatively new field of research, and not enough preclinical studies have been conducted yet. The earlier developed, larger gold nanoparticles have been under investigation in clinical trials for several years already.<sup>118</sup> Considering the current drawbacks of gold nanoparticles, mainly caused by controversial and inconsistent outcomes *in vitro* and *in vivo*, one could argue for the superiority of AuNCs. Whereas some gold nanoparticles can exhibit disadvantages including toxicity, species-specific differences in biodistribution and physiological response, relatively large size, and RES organ accumulation,<sup>118</sup> AuNCs presented so far show little to no inherent toxicity, good biocompatibility, satisfactory biodistribution, and renal clearance. Depending on the capping-ligand, the cellular uptake efficiency and clearance are either improved or decreased. In general, AuNCs accumulate well in cells via endocytic pathways.<sup>107</sup> A set of experiments comparing the clearance of AuNCs and gold nanoparticles concluded that the size of the AuNCs is an advantage here.<sup>84</sup> Using the same capping ligand, targeting agent, and amount of gold, the gold nanoparticles accumulated twice as much in the liver compared to the AuNCs.<sup>84</sup> In addition to that, earlier obtained results from Tsvirkun et al. in 2018 stated that they found a reverse correlation between gold nanoparticle size and tumor uptake via CT imaging.<sup>119</sup> From these studies, a careful conclusion could be drawn that the AuNCs can be superior to the larger gold nanoparticles for cancer therapy applications *in vivo* with regard to tumor uptake, toxicity, biodistribution, and clearance, which could contribute to improved treatment outcomes.

In other fields, AuNCs and gold nanoparticles compare well. With the appropriate surface modifications, gold nanoparticles too can cross the BBB.<sup>118</sup> AuNCs have been found to do this because of their small size.<sup>116</sup> They can also both be used for applications in drug delivery, active targeting, photothermal and photodynamic therapy (usually with conjugated photosensitizer), and CT imaging.<sup>118</sup>

Another feature of AuNCs is that they can be used for various applications such as the sensing of heavy metals, biological molecules, and intracellular temperature. Even in surgery, the AuNCs may be of use, for example, in robot-assisted fluorescence-guided surgery. Furthermore, the use of



AuNCs (among other metal nanoclusters) as bactericidal agents has also gained increasing interest.<sup>120</sup>

However, it is imperative to look at both sides of the coin, as there are limits to the use of AuNCs as diagnostic and therapeutic agents as well. One example is the limitations that arise from the AuNCs' native fluorescence peaks being most commonly in the NIR range. Deep tissue imaging (imaging with a depth from millimeters to centimeters) requires imaging wavelengths between 650 and 900 nm, because then only little amounts of absorption from water and blood occur.<sup>121</sup> Nevertheless, the window is not optimal either because of autofluorescence of tissues that cause some background noise. So, even though the tissue penetration of NIR-I and NIR-II light is better than that of visible light and UV-light, the imaging capability is not deeper than 1 or 2 cm.<sup>122</sup> This is in contrast to other imaging techniques that are currently in use for the purpose of diagnostics. CT, MRI, and PET imaging have unlimited tissue penetration, but they each have their own shortcomings.<sup>123</sup> Major limitations of CT are that it uses ionizing radiation and that it has a low soft tissue sensitivity. MRI has a high spatial resolution but has the disadvantage that the overall sensitivity is low. PET imaging, on the other hand, has excellent sensitivity, but is very costly and has a low spatial resolution.<sup>123</sup> When applying NIR-fluorescent imaging alone, not enough functional information can be obtained. However, multimodal fluorescent imaging, where fluorescence imaging is combined with other imaging possibilities, has emerged as a promising tool for imaging with improved sensitivity and accuracy.<sup>123</sup> Considering that AuNCs have already been researched for multimodal fluorescent imaging, the limitations of NIR light may be overcome.

Currently, indocyanine green is the only fluorescent dye approved by the FDA for clinical use. The IRDye 800CW has entered clinical trials conjugated to antibodies, thus as targeted tracers.<sup>123,124</sup> These dyes have a slight advantage over NIR-fluorescent AuNCs in the way that they also emit light with a high intensity in the NIR-II window, providing a higher imaging contrast and even deeper tissue penetration.<sup>125</sup> However, without coupling them to another functionality, they do not have the possibility for multimodal imaging.

Another, perhaps more important, aspect of AuNCs that may hinder their progress to human studies is that GSH-capped AuNCs may cause epigenetic modifications in healthy cells at non-cytotoxic levels.<sup>126</sup> The notion that they have a direct effect on epigenetic processes could cause unwanted side-effects during diagnosis or treatment. Still, as far as our knowledge goes, it has only been reported once and should thus be investigated more in-depth before drawing conclusions.

As illustrated in this review, various biomolecules (including peptides and proteins) as well as various other materials such as polymers may be employed as capping ligands for AuNCs. This provides opportunities for reducing toxicity, improving biocompatibility and targeting, which ultimately make AuNCs an attractive and versatile tool for biomedical applications.<sup>127,128</sup> Furthermore, the increase in AuNC related publications over the last 15 years for imaging, sensing, and therapy speaks volumes toward the increased interest for AuNCs in biomedical applications, increasing confidence that clinical translation may not be too far off anymore.<sup>129–132</sup>

## 7. FUTURE PERSPECTIVES

All in all, while promising research focused on enabling the use of the emergent properties of AuNCs that have been

developed, translation of this laboratory knowledge to functional clinical technology will take time. To efficiently image cancer tissue, employing targeting ligands such as folic acid, hyaluronic acid, or the aptamer AS1411 on the surface has been shown to improve uptake in tumor cells by active targeting. By means of fluorescence imaging and CT imaging, tumors can then be diagnosed accurately. With only minor modifications to the surface chemistry, PET and MRI are also within reach. Ideally, the AuNC-containing system would be used for diagnosis first, before locally activating treatment. This would reduce side-effects while providing a highly efficient solution to inhibit tumor growth. In this regard, acid-, enzyme-, or redox-sensitive linkers can help pave the way toward achieving localized release. Drug-release or therapy triggered by external factors, such as local light activation with a (NIR-)laser, could also be a solution for this. Additionally, photothermal, photodynamic, and radiation therapy may also serve as alternative therapies in different combinations. For the application of photothermal therapy, a balance should be found between photoluminescence and photothermal conversion for optimal results. In the end, the most powerful theranostic approach would consist of both multimodal imaging and combination therapy. Perhaps one day, AuNCs will be the new golden standard in the diagnosis and treatment of cancer or other newly emerging fields of application in infectious diseases and neurological disorders.

## AUTHOR INFORMATION

### Corresponding Author

**Tina Vermonden** – Department of Pharmaceutics, Utrecht Institute for Pharmaceutical Sciences (UIPS), Science for Life, Utrecht University, 3508 TB Utrecht, The Netherlands; [orcid.org/0000-0002-6047-5900](https://orcid.org/0000-0002-6047-5900); Email: [T.Vermonden@uu.nl](mailto:T.Vermonden@uu.nl)

### Authors

**Sanne M. van de Looij** – Department of Pharmaceutics, Utrecht Institute for Pharmaceutical Sciences (UIPS), Science for Life, Utrecht University, 3508 TB Utrecht, The Netherlands

**Erik R. Hebels** – Department of Pharmaceutics, Utrecht Institute for Pharmaceutical Sciences (UIPS), Science for Life, Utrecht University, 3508 TB Utrecht, The Netherlands

**Martina Viola** – Department of Pharmaceutics, Utrecht Institute for Pharmaceutical Sciences (UIPS), Science for Life, Utrecht University, 3508 TB Utrecht, The Netherlands

**Mathew Hembury** – Department of Pharmaceutics, Utrecht Institute for Pharmaceutical Sciences (UIPS), Science for Life, Utrecht University, 3508 TB Utrecht, The Netherlands

**Sabrina Oliveira** – Department of Pharmaceutics, Utrecht Institute for Pharmaceutical Sciences (UIPS), Science for Life and Department of Biology, Cell Biology, Neurobiology and Biophysics, Faculty of Science, Utrecht University, 3508 TB Utrecht, The Netherlands; [orcid.org/0000-0002-6011-2122](https://orcid.org/0000-0002-6011-2122)

Complete contact information is available at: <https://pubs.acs.org/10.1021/acs.bioconjchem.1c00475>

### Author Contributions

#S.N. van de Looij and E.R. Hebels contributed equally to the work

### Notes

The authors declare no competing financial interest.



## ACKNOWLEDGMENTS

The Netherlands Organization for Scientific Research (NWO/Aspasia 015.009.038 and NWO/Industrial Doctorates NWA.ID.17.030) is acknowledged for funding.

## ABBREVIATIONS LIST

AcSEMA, 2-(Aethylthio)ethyl methacrylate; APC, Antigen presenting cells; ATP, Adenosine triphosphate; AuNC, Gold nanocluster; BBB, Blood brain barrier; BSA, Bovine serum albumin; CAT, Catalase; CNS, Central nervous system; CpG, Cytosine-phosphate-guanine; CT, Computed tomography; CY, Cysteine; DC, Dendritic cells; DNA, Deoxyribose nucleic acid; DOX, Doxorubicin; DOX-SH, Doxorubicin-iminothiolane; EGCG, Epigallocatechin gallate; EGFR, Epidermal growth factor receptor; EPR, Enhanced permeability and retention; FA, Folic acid; FDA, Food and Drug Administration; FLIM, Fluorescence lifetime imaging microscopy; GFP, Green fluorescent protein; GPM, Poly(ethylene glycol)-*b*-poly( $\epsilon$ -caprolactone) micelles containing AuNCs; GPPS, Sulfated polysaccharide; GSH, Glutathione; HA, Hyaluronic acid; HEVA, Hepatitis E vaccine; HNSCC, Head and neck squamous cell carcinoma; HSA, Human serum albumin; IC50, Inhibiting concentration 50%; ICG, Indocyanine green; IgG, Immunoglobulin G; IL, Interleukin; IV, Intravenous; L-NIBC, N-isobutyryl-L-cysteine; LOD, Limit of detection; Lys, Lysozyme; MDR, Multidrug resistant; MMP2, Matrix metalloproteinase-2; MPA, Quadrupolar anthracene-based dye; MRI, Magnetic resonance imaging; MRSA, Methicillin-resistant *S. aureus*; NADP<sup>+</sup>, Nicotinamide adenine dinucleotide phosphate; NGF, Nerve growth factor; NIR, Near infrared; NIR-II, NIR light in the second biological window between 1000 and 1400 nm; ODN, Oligodeoxynucleotides; OEGMA, Oligo(ethylene glycol) methyl ether methacrylate; PAL, Photoacoustic imaging; PAMAM, Poly(amidoamine) dendrimer; PBS, Phosphate buffered saline; PCR, Polymerase chain reaction; PD, Parkinson's disease; PDT, Photodynamic therapy; PEG, Poly(ethylene glycol); PEI, Polyethylenimine; PET, Positron emission tomography; PLA, Poly(L-lactide); PMMA, Poly(methyl methacrylate); PNIPAM, Poly(*N*-isopropylacrylamide); PSMA, Prostate specific membrane antigen; PTEN, Phosphatase and tensin homologue tumor suppressor gene; PTT, Photothermal therapy; PVP, Poly(*N*-vinylpyrrolidone); QA, Quaternary ammonium; QY, Luminescence quantum yield; RES, Reticuloendothelial system; RGD, Arginine-glycine-aspartic acid; RNA, Ribonucleic acid; ROS, Reactive oxygen species; siRNA, Small interfering RNA; SWIR, Short wavelength infrared; TNF- $\alpha$ , Tumor necrosis factor; TPGS, Vitamin E tocopheryl polyethylene glycol 1000 succinate; Try, Trypsin; UV, Ultraviolet; VEGFR, Vascular epidermal growth factor receptor; VRE, Vancomycin-resistant *Enterococci*

## REFERENCES

- (1) Li, H.; Li, H.; Wan, A. Luminescent Gold Nanoclusters for in Vivo Tumor Imaging. *Analyst* **2020**, *145* (2), 348–363.
- (2) Siegel, R. L.; Miller, K. D.; Jemal, A. Cancer Statistics, 2019. *Ca-Cancer J. Clin.* **2019**, *69* (1), 7–34.
- (3) Soper, S. A.; Rasooly, A. Cancer: A Global Concern That Demands New Detection Technologies. *Analyst* **2016**, *141* (2), 367–370.
- (4) Zhang, Q.; Yang, M.; Zhu, Y.; Mao, C. Metallic Nanoclusters for Cancer Imaging and Therapy. *Curr. Med. Chem.* **2018**, *25*, 1379.
- (5) Zheng, Y.; Wu, J.; Jiang, H.; Wang, X. Gold Nanoclusters for Theranostic Applications. *Coord. Chem. Rev.* **2021**, *431*, 213689.
- (6) Hembury, M.; Beztsinna, N.; Asadi, H.; Van Den Dikkenberg, J. B.; Meeldijk, J. D.; Hennink, W. E.; Vermonden, T. Luminescent Gold Nanocluster-Decorated Polymeric Hybrid Particles with Assembly-Induced Emission. *Biomacromolecules* **2018**, *19* (7), 2841–2848.
- (7) Jin, R. Quantum Sized, Thiolate-Protected Gold Nanoclusters. *Nanoscale* **2010**, *2* (3), 343–362.
- (8) Cantelli, A.; Battistelli, G.; Guidetti, G.; Manzi, J.; Di Giosia, M.; Montalti, M. Luminescent Gold Nanoclusters as Biocompatible Probes for Optical Imaging and Theranostics. *Dyes Pigm.* **2016**, *135*, 64–79.
- (9) Yang, T.-Q.; Peng, B.; Shan, B.-Q.; Zong, Y.-X.; Jiang, J.-G.; Wu, P.; Zhang, K. Origin of the Photoluminescence of Metal Nanoclusters: From Metal-Centered Emission to Ligand-Centered Emission. *Nanomaterials* **2020**, *10* (2), 261.
- (10) Wu, Z.; Jin, R. On the Ligand's Role in the Fluorescence of Gold Nanoclusters. *Nano Lett.* **2010**, *10* (7), 2568–2573.
- (11) Hebels, E. R.; Najafi, M.; van den Dikkenberg, J.; Beztsinna, N.; van de Looij, S.; Wilbie, D.; Meeldijk, J.; Hembury, M.; Vermonden, T. Luminescent Gold Nanocluster-Decorated Polymeric Hybrid Particles for Laser Guided Therapy. *Eur. Polym. J.* **2021**, *152*, 110467.
- (12) Yu, N.; Huang, L.; Zhou, Y.; Xue, T.; Chen, Z.; Han, G. Near-Infrared-Light Activatable Nanoparticles for Deep-Tissue-Penetrating Wireless Optogenetics. *Adv. Healthcare Mater.* **2019**, *8* (6), 1801132.
- (13) Chen, L.-Y.; Wang, C.-W.; Yuan, Z.; Chang, H.-T. Fluorescent Gold Nanoclusters: Recent Advances in Sensing and Imaging. *Anal. Chem.* **2015**, *87* (1), 216–229.
- (14) Kelkar, S. S.; Reineke, T. M. Theranostics: Combining Imaging and Therapy. *Bioconjugate Chem.* **2011**, *22* (10), 1879–1903.
- (15) Cheng, Y.; Lu, G.; He, Y.; Shen, H.; Zhao, J.; Xia, K.; Gong, Q. Luminescence Quantum Yields of Gold Nanoparticles Varying with Excitation Wavelengths. *Nanoscale* **2016**, *8* (4), 2188–2194.
- (16) Chistopoulos, T. K.; Diamandis, E. P. Fluorescence Immunoassays. In *Immunoassay*; Elsevier, 1996; pp 309–335. DOI: 10.1016/B978-012214730-2/S0015-7.
- (17) Zhang, X. D.; Wu, D.; Shen, X.; Liu, P. X.; Fan, F. Y.; Fan, S. J. In Vivo Renal Clearance, Biodistribution, Toxicity of Gold Nanoclusters. *Biomaterials* **2012**, *33* (18), 4628–4638.
- (18) Xie, J.; Zheng, Y.; Ying, J. Y. Protein-Directed Synthesis of Highly Fluorescent Gold Nanoclusters. *J. Am. Chem. Soc.* **2009**, *131* (3), 888–889.
- (19) Wang, J.; Ma, S.; Ren, J.; Yang, J.; Qu, Y.; Ding, D.; Zhang, M.; Yang, G. Fluorescence Enhancement of Cysteine-Rich Protein-Templated Gold Nanoclusters Using Silver(I) Ions and Its Sensing Application for Mercury(II). *Sens. Actuators, B* **2018**, *267*, 342–350.
- (20) Wang, Y.; Chen, J. T.; Yan, X. P. Fabrication of Transferrin Functionalized Gold Nanoclusters/Graphene Oxide Nanocomposite for Turn-on near-Infrared Fluorescent Bioimaging of Cancer Cells and Small Animals. *Anal. Chem.* **2013**, *85* (4), 2529–2535.
- (21) Chen, T.-H.; Tseng, W.-L. (Lysozyme Type VI)-Stabilized Au8 Clusters: Synthesis Mechanism and Application for Sensing of Glutathione in a Single Drop of Blood. *Small* **2012**, *8* (12), 1912–1919.
- (22) Wei, H.; Wang, Z.; Yang, L.; Tian, S.; Hou, C.; Lu, Y. Lysozyme-Stabilized Gold Fluorescent Cluster: Synthesis and Application as Hg<sup>2+</sup> Sensor. *Analyst* **2010**, *135* (6), 1406.
- (23) Li, Y.; Cao, Y.; Wei, L.; Wang, J.; Zhang, M.; Yang, X.; Wang, W.; Yang, G. The Assembly of Protein-Templated Gold Nanoclusters for Enhanced Fluorescence Emission and Multifunctional Applications. *Acta Biomater.* **2020**, *101*, 436–443.
- (24) Kawasaki, H.; Hamaguchi, K.; Osaka, I.; Arakawa, R. pH-Dependent Synthesis of Pepsin-Mediated Gold Nanoclusters with Blue Green and Red Fluorescent Emission. *Adv. Funct. Mater.* **2011**, *21* (18), 3508–3515.
- (25) Liu, C.-L.; Wu, H.-T.; Hsiao, Y.-H.; Lai, C.-W.; Shih, C.-W.; Peng, Y.-K.; Tang, K.-C.; Chang, H.-W.; Chien, Y.-C.; Hsiao, J.-K.; Cheng, J.-T.; Chou, P.-T. Insulin-Directed Synthesis of Fluorescent

- Gold Nanoclusters: Preservation of Insulin Bioactivity and Versatility in Cell Imaging. *Angew. Chem., Int. Ed.* **2011**, *50* (31), 7056–7060.
- (26) Kong, Y.; Chen, J.; Gao, F.; Brydson, R.; Johnson, B.; Heath, G.; Zhang, Y.; Wu, L.; Zhou, D. Near-Infrared Fluorescent Ribonuclease-A-Encapsulated Gold Nanoclusters: Preparation, Characterization, Cancer Targeting and Imaging. *Nanoscale* **2013**, *5* (3), 1009–1017.
- (27) West, A. L.; Griep, M. H.; Cole, D. P.; Karna, S. P. DNase I Retains Endonuclease Activity Following Gold Nanocluster Synthesis. *Anal. Chem.* **2014**, *86* (15), 7377–7382.
- (28) Wen, F.; Dong, Y.; Feng, L.; Wang, S.; Zhang, S.; Zhang, X. Horseradish Peroxidase Functionalized Fluorescent Gold Nanoclusters for Hydrogen Peroxide Sensing. *Anal. Chem.* **2011**, *83* (4), 1193–1196.
- (29) Xu, Y.; Sherwood, J.; Qin, Y.; Crowley, D.; Bonizzoni, M.; Bao, Y. The Role of Protein Characteristics in the Formation and Fluorescence of Au Nanoclusters. *Nanoscale* **2014**, *6* (3), 1515–1524.
- (30) Chen, Y.; Montana, D. M.; Wei, H.; Cordero, J. M.; Schneider, M.; Le Guével, X.; Chen, O.; Bruns, O. T.; Bawendi, M. G. Shortwave Infrared in Vivo Imaging with Gold Nanoclusters. *Nano Lett.* **2017**, *17* (10), 6330–6334.
- (31) Lopez, A.; Liu, J. DNA-Templated Fluorescent Gold Nanoclusters Reduced by Good's Buffer: From Blue-Emitting Seeds to Red and near Infrared Emitters. *Can. J. Chem.* **2015**, *93* (6), 615–620.
- (32) Zhou, C.; Long, M.; Qin, Y.; Sun, X.; Zheng, J. Luminescent Gold Nanoparticles with Efficient Renal Clearance. *Angew. Chem., Int. Ed.* **2011**, *50* (14), 3168–3172.
- (33) Luo, Z.; Yuan, X.; Yu, Y.; Zhang, Q.; Leong, D. T.; Lee, J. Y.; Xie, J. From Aggregation-Induced Emission of Au(I)–Thiolate Complexes to Ultrabright Au(0)@Au(I)–Thiolate Core–Shell Nanoclusters. *J. Am. Chem. Soc.* **2012**, *134* (40), 16662–16670.
- (34) Bera, D.; Goswami, N. Driving Forces and Routes for Aggregation-Induced Emission-Based Highly Luminescent Metal Nanocluster Assembly. *J. Phys. Chem. Lett.* **2021**, *12* (37), 9033–9046.
- (35) Zheng, J.; Zhang, C.; Dickson, R. M. Highly Fluorescent, Water-Soluble, Size-Tunable Gold Quantum Dots. *Phys. Rev. Lett.* **2004**, *93* (7), 1 DOI: 10.1103/PhysRevLett.93.077402.
- (36) Santiago González, B.; Rodríguez, M. J.; Blanco, C.; Rivas, J.; López-Quintela, M. A.; Martinho, J. M. G. One Step Synthesis of the Smallest Photoluminescent and Paramagnetic PVP-Protected Gold Atomic Clusters. *Nano Lett.* **2010**, *10* (10), 4217–4221.
- (37) Duan, H.; Nie, S. Etching Colloidal Gold Nanocrystals with Hyperbranched and Multivalent Polymers: A New Route to Fluorescent and Water-Soluble Atomic Clusters. *J. Am. Chem. Soc.* **2007**, *129* (9), 2412–2413.
- (38) Hussain, I.; Graham, S.; Wang, Z.; Tan, B.; Sherrington, D. C.; Rannard, S. P.; Cooper, A. I.; Brust, M. Size-Controlled Synthesis of Near-Monodisperse Gold Nanoparticles in the 1–4 Nm Range Using Polymeric Stabilizers. *J. Am. Chem. Soc.* **2005**, *127* (47), 16398–16399.
- (39) Adnan, N. N. M.; Ahmad, S.; Kuchel, R. P.; Boyer, C. Exploring the Potential of Linear Polymer Structures for the Synthesis of Fluorescent Gold Nanoclusters. *Mater. Chem. Front.* **2017**, *1* (1), 80–90.
- (40) Al Zaki, A.; Joh, D.; Cheng, Z.; De Barros, A. L. B.; Kao, G.; Dorsey, J.; Tsourkas, A. Gold-Loaded Polymeric Micelles for Computed Tomography-Guided Radiation Therapy Treatment and Radiosensitization. *ACS Nano* **2014**, *8* (1), 104–112.
- (41) Chen, D.; Luo, Z.; Li, N.; Lee, J. Y.; Xie, J.; Lu, J. Amphiphilic Polymeric Nanocarriers with Luminescent Gold Nanoclusters for Concurrent Bioimaging and Controlled Drug Release. *Adv. Funct. Mater.* **2013**, *23* (35), 4324–4331.
- (42) Ma, H.; Wang, J.; Zhang, X. D. Near-Infrared II Emissive Metal Clusters: From Atom Physics to Biomedicine. *Coord. Chem. Rev.* **2021**, *448*, 214184.
- (43) Liu, H.; Hong, G.; Luo, Z.; Chen, J.; Chang, J.; Gong, M.; He, H.; Yang, J.; Yuan, X.; Li, L.; Mu, X.; Wang, J.; Mi, W.; Luo, J.; Xie, J.; Zhang, X. Atomic-Precision Gold Clusters for NIR-II Imaging. *Adv. Mater.* **2019**, *31* (46), 1901015.
- (44) Porret, E.; Le Guével, X.; Coll, J.-L. Gold Nanoclusters for Biomedical Applications: Toward in Vivo Studies. *J. Mater. Chem. B* **2020**, *8* (11), 2216–2232.
- (45) Talelli, M.; Barz, M.; Rijcken, C. J. F.; Kiessling, F.; Hennink, W. E.; Lammers, T. Core-Crosslinked Polymeric Micelles: Principles, Preparation, Biomedical Applications and Clinical Translation. *Nano Today* **2015**, *10* (1), 93–117.
- (46) Torchilin, V. Tumor Delivery of Macromolecular Drugs Based on the EPR Effect. *Adv. Drug Delivery Rev.* **2011**, *63* (3), 131–135.
- (47) Liu, J. M.; Chen, J. T.; Yan, X. P. Near Infrared Fluorescent Trypsin Stabilized Gold Nanoclusters as Surface Plasmon Enhanced Energy Transfer Biosensor and in Vivo Cancer Imaging Bioprobe. *Anal. Chem.* **2013**, *85* (6), 3238–3245.
- (48) Zhang, P.; Yang, X. X.; Wang, Y.; Zhao, N. W.; Xiong, Z. H.; Huang, C. Z. Rapid Synthesis of Highly Luminescent and Stable Au20 Nanoclusters for Active Tumor-Targeted Imaging in Vitro and in Vivo. *Nanoscale* **2014**, *6* (4), 2261–2269.
- (49) Hembury, M.; Chiappini, C.; Bertazzo, S.; Kalber, T. L.; Drisko, G. L.; Ogunlade, O.; Walker-Samuel, S.; Krishna, K. S.; Jumeaux, C.; Beard, P.; Kumar, C. S. S. R.; Porter, A. E.; Lythgoe, M. F.; Boissière, C.; Sanchez, C.; Stevens, M. M. Gold–Silica Quantum Rattles for Multimodal Imaging and Therapy. *Proc. Natl. Acad. Sci. U. S. A.* **2015**, *112* (7), 1959–1964.
- (50) Han, W.; Yang, W.; Gao, F.; Cai, P.; Wang, J.; Wang, S.; Xue, J.; Gao, X.; Liu, Y. Iodine-124 Labeled Gold Nanoclusters for Positron Emission Tomography Imaging in Lung Cancer Model. *J. Nanosci. Nanotechnol.* **2020**, *20* (3), 1375–1382.
- (51) Liu, Y.; Tian, G. F.; He, X. W.; Li, W. Y.; Zhang, Y. K. Microwave-Assisted One-Step Rapid Synthesis of near-Infrared Gold Nanoclusters for NIRF/CT Dual-Modal Bioimaging. *J. Mater. Chem. B* **2016**, *4* (7), 1276–1283.
- (52) Hu, D. H.; Sheng, Z. H.; Zhang, P. F.; Yang, D. Z.; Liu, S. H.; Gong, P.; Gao, D. Y.; Fang, S. T.; Ma, Y. F.; Cai, L. T. Hybrid Gold-Gadolinium Nanoclusters for Tumor-Targeted NIRF/CT/MRI Triple-Modal Imaging in Vivo. *Nanoscale* **2013**, *5* (4), 1624–1628.
- (53) Zhang, H.; Han, W.; Cao, X.; Gao, T.; Jia, R.; Liu, M.; Zeng, W. Gold Nanoclusters as a Near-Infrared Fluorometric Nanothermometer for Living Cells. *Microchim. Acta* **2019**, *186* (6), 1–6.
- (54) Yang, L.; Lou, X.; Yu, F.; Liu, H. Cross-Linking Structure-Induced Strong Blue Emissive Gold Nanoclusters for Intracellular Sensing. *Analyst* **2019**, *144* (8), 2765–2772.
- (55) Shang, L.; Stockmar, F.; Azadfar, N.; Nienhaus, G. U. Intracellular Thermometry by Using Fluorescent Gold Nanoclusters. *Angew. Chem., Int. Ed.* **2013**, *52* (42), 11154–11157.
- (56) Wang, X. D.; Wolfbeis, O. S.; Meier, R. J. Luminescent Probes and Sensors for Temperature. *Chem. Soc. Rev.* **2013**, *42* (19), 7834–7869.
- (57) Donner, J. S.; Thompson, S. A.; Kreuzer, M. P.; Baffou, G.; Quidant, R. Mapping Intracellular Temperature Using Green Fluorescent Protein. *Nano Lett.* **2012**, *12* (4), 2107–2111.
- (58) Selvaprakash, K.; Chen, Y. C. Using Protein-Encapsulated Gold Nanoclusters as Photoluminescent Sensing Probes for Biomolecules. *Biosens. Bioelectron.* **2014**, *61*, 88–94.
- (59) Xia, X.; Long, Y.; Wang, J. Glucose Oxidase-Functionalized Fluorescent Gold Nanoclusters as Probes for Glucose. *Anal. Chim. Acta* **2013**, *772*, 81–86.
- (60) Peng, J.; Feng, L.-N.; Zhang, K.; Li, X.-H.; Jiang, L.-P.; Zhu, J.-J. Calcium Carbonate-Gold Nanocluster Hybrid Spheres: Synthesis and Versatile Application in Immunoassays. *Chem. - Eur. J.* **2012**, *18* (17), 5261–5268.
- (61) Govindaraju, S.; Ankireddy, S. R.; Viswanath, B.; Kim, J.; Yun, K. Fluorescent Gold Nanoclusters for Selective Detection of Dopamine in Cerebrospinal Fluid. *Sci. Rep.* **2017**, *7* (1), 1–12.
- (62) Yang, G. H.; Shi, J. J.; Wang, S.; Xiong, W. W.; Jiang, L. P.; Burda, C.; Zhu, J. J. Fabrication of a Boron Nitride-Gold Nanocluster Composite and Its Versatile Application for Immunoassays. *Chem. Commun.* **2013**, *49* (91), 10757–10759.



- (63) Liu, Q.; Na, W.; Wang, L.; Su, X. Gold Nanocluster-Based Fluorescent Assay for Label-Free Detection of Protein Kinase and Its Inhibitors. *Micromol. Acta* **2017**, *184* (9), 3381–3387.
- (64) Colombé, C.; Le Guével, X.; Martin-Serrano, A.; Henry, M.; Porret, E.; Comby-Zerbino, C.; Antoine, R.; Atallah, I.; Busser, B.; Coll, J.-L.; Righini, C. A.; Sancey, L. Gold Nanoclusters as a Contrast Agent for Image-Guided Surgery of Head and Neck Tumors. *Nanomedicine* **2019**, *20*, 102011.
- (65) Atallah, I.; Milet, C.; Henry, M.; Jossierand, V.; Reyt, E.; Coll, J.-L.; Hurbin, A.; Righini, C. A. Near-Infrared Fluorescence Imaging-Guided Surgery Improves Recurrence-Free Survival Rate in Novel Orthotopic Animal Model of Head and Neck Squamous Cell Carcinoma. *Head Neck* **2016**, *38* (S1), E246–E255.
- (66) De Boer, E.; Warram, J. M.; Tucker, M. D.; Hartman, Y. E.; Moore, L. S.; De Jong, J. S.; Chung, T. K.; Korb, M. L.; Zinn, K. R.; Van Dam, G. M.; Rosenthal, E. L.; Brandwein-Gensler, M. S. In Vivo Fluorescence Immunohistochemistry: Localization of Fluorescently Labeled Cetuximab in Squamous Cell Carcinomas. *Sci. Rep.* **2015**, *5* (1), 1–11.
- (67) Hernot, S.; van Manen, L.; Debie, P.; Mieog, J. S. D.; Vahrmeijer, A. L. Latest Developments in Molecular Tracers for Fluorescence Image-Guided Cancer Surgery. *Lancet Oncol.* **2019**, *20* (7), e354–e367.
- (68) Cui, H.; Shao, Z.-S.; Song, Z.; Wang, Y.-B.; Wang, H.-S. Development of Gold Nanoclusters: From Preparation to Applications in the Field of Biomedicine. *J. Mater. Chem. C* **2020**, *8* (41), 14312–14333.
- (69) Sood, K.; Shanavas, A. The Role of Gold Nanoclusters as Emerging Theranostic Agents for Cancer Management. *Curr. Pathobiol. Rep.* **2021**, *9* (2), 33–42.
- (70) Sonia; Komal; Kukreti, S.; Kaushik, M. Gold Nanoclusters: An Ultrasmall Platform for Multifaceted Applications. *Talanta* **2021**, *122* (March), 122623.
- (71) Karaki, N.; Ali, H. H.; El Kak, A. Gold Nanoparticles as Promising Agents for Cancer Therapy. In *Nanoparticle Drug Delivery Systems for Cancer Treatment*, Gali-Muhtasib, H.; Chouaib, R., Eds.; Jenny Stanford Publishing: Singapore, 2020; pp 235–270. DOI: 10.1201/9780429341250-9.
- (72) Liu, P.; Yang, W.; Shi, L.; Zhang, H.; Xu, Y.; Wang, P.; Zhang, G.; Chen, W. R.; Zhang, B.; Wang, X. Concurrent Photothermal Therapy and Photodynamic Therapy for Cutaneous Squamous Cell Carcinoma by Gold Nanoclusters under a Single NIR Laser Irradiation. *J. Mater. Chem. B* **2019**, *7* (44), 6924–6933.
- (73) Melamed, J. R.; Edelstein, R. S.; Day, E. S. Elucidating the Fundamental Mechanisms of Cell Death Triggered by Photothermal Therapy. *ACS Nano* **2015**, *9* (1), 6–11.
- (74) Kim, J.; Piao, Y.; Hyeon, T. Multifunctional Nanostructured Materials for Multimodal Imaging, and Simultaneous Imaging and Therapy. *Chem. Soc. Rev.* **2009**, *38* (2), 372–390.
- (75) Bettaieb, A. Hyperthermia: Cancer Treatment and Beyond. In *Cancer Treatment - Conventional and Innovative Approaches*; IntechOpen: London, UK, 2013; pp 257–283. DOI: 10.5772/55795.
- (76) Chen, Q.; Wang, C.; Zhan, Z.; He, W.; Cheng, Z.; Li, Y.; Liu, Z. Near-Infrared Dye Bound Albumin with Separated Imaging and Therapy Wavelength Channels for Imaging-Guided Photothermal Therapy. *Biomaterials* **2014**, *35* (28), 8206–8214.
- (77) Morton, C.; Szeimies, R. M.; Sidoroff, A.; Wennberg, A. M.; Basset-Seguín, N.; Calzavara-Pinton, P.; Gilaberte, Y.; Hofbauer, G.; Hunger, R.; Karrer, S.; Lehmann, P.; Piaserico, S.; Ulrich, C.; Braathen, L. European Dermatology Forum Guidelines on Topical Photodynamic Therapy. *Eur. J. Dermatol.* **2015**, *25* (4), 296–311.
- (78) Bhandari, C.; Guirguis, M.; Savan, N. A.; Shrivastava, N.; Oliveira, S.; Hasan, T.; Obaid, G. What NIR Photodynamic Activation Offers Molecular Targeted Nanomedicines: Perspectives into the Conundrum of Tumor Specificity and Selectivity. *Nano Today* **2021**, *36*, 101052.
- (79) Chen, Q.; Chen, J.; Yang, Z.; Zhang, L.; Dong, Z.; Liu, Z. NIR-II Light Activated Photodynamic Therapy with Protein-Capped Gold Nanoclusters. *Nano Res.* **2018**, *11* (10), 5657–5669.
- (80) Liu, C.-P.; Wu, T.-H.; Liu, C.-Y.; Chen, K.-C.; Chen, Y.-X.; Chen, G.-S.; Lin, S.-Y. Self-Supplying O<sub>2</sub> through the Catalase-Like Activity of Gold Nanoclusters for Photodynamic Therapy against Hypoxic Cancer Cells. *Small* **2017**, *13* (26), 1700278.
- (81) Liang, G.; Jin, X.; Zhang, S.; Xing, D. RGD Peptide-Modified Fluorescent Gold Nanoclusters as Highly Efficient Tumor-Targeted Radiotherapy Sensitizers. *Biomaterials* **2017**, *144*, 95–104.
- (82) Su, Y.; Xue, T.; Liu, Y.; Qi, J.; Jin, R.; Lin, Z. Luminescent Metal Nanoclusters for Biomedical Applications. *Nano Res.* **2019**, *12* (6), 1251–1265.
- (83) Zhang, X.-D.; Chen, J.; Luo, Z.; Wu, D.; Shen, X.; Song, S.-S.; Sun, Y.-M.; Liu, P.-X.; Zhao, J.; Huo, S.; Fan, S.; Fan, F.; Liang, X.-J.; Xie, J. Enhanced Tumor Accumulation of Sub-2 Nm Gold Nanoclusters for Cancer Radiation Therapy. *Adv. Healthcare Mater.* **2014**, *3* (1), 133–141.
- (84) Luo, D.; Wang, X.; Zeng, S.; Ramamurthy, G.; Burda, C.; Basilion, J. P. Targeted Gold Nanocluster-Enhanced Radiotherapy of Prostate Cancer. *Small* **2019**, *15* (34), 1900968.
- (85) De Jong, W. H.; Hagens, W. I.; Krystek, P.; Burger, M. C.; Sips, A. J. A. M.; Geertsma, R. E. Particle Size-Dependent Organ Distribution of Gold Nanoparticles after Intravenous Administration. *Biomaterials* **2008**, *29* (12), 1912–1919.
- (86) Ghahremani, F.; Shahbazi-Gahrouei, D.; Kefayat, A.; Motaghi, H.; Mehrgardi, M. A.; Javanmard, S. H. AS1411 Aptamer Conjugated Gold Nanoclusters as a Targeted Radiosensitizer for Megavoltage Radiation Therapy of 4T1 Breast Cancer Cells. *RSC Adv.* **2018**, *8* (8), 4249–4258.
- (87) Cifuentes-Rius, A.; Ivask, A.; Das, S.; Penya-Auladell, N.; Fabregas, L.; Fletcher, N. L.; Houston, Z. H.; Thurecht, K. J.; Voelcker, N. H. Gold Nanocluster-Mediated Cellular Death under Electromagnetic Radiation. *ACS Appl. Mater. Interfaces* **2017**, *9* (47), 41159–41167.
- (88) Govindaraju, S.; Roshini, A.; Lee, M.-H.; Yun, K. Kaempferol Conjugated Gold Nanoclusters Enabled Efficient for Anticancer Therapeutics to A549 Lung Cancer Cells. *Int. J. Nanomed.* **2019**, *14*, 5147–5157.
- (89) Govindaraju, S.; Rengaraj, A.; Arivazhagan, R.; Huh, Y. S.; Yun, K. Curcumin-Conjugated Gold Clusters for Bioimaging and Anticancer Applications. *Bioconjugate Chem.* **2018**, *29* (2), 363–370.
- (90) Fu, C.; Ding, C.; Sun, X.; Fu, A. Curcumin Nanocapsules Stabilized by Bovine Serum Albumin-Capped Gold Nanoclusters (BSA-AuNCs) for Drug Delivery and Theranosis. *Mater. Sci. Eng., C* **2018**, *87*, 149–154.
- (91) Lakshmi, B. A.; Kim, S. Quercetin Mediated Gold Nanoclusters Explored as a Dual Functional Nanomaterial in Anticancer and Bio-Imaging Disciplines. *Colloids Surf., B* **2019**, *178*, 230–237.
- (92) Latorre; Latorre; Castellanos; Diaz; Lazaro-Carrillo; Aguado; Lecea; Romero-Pérez; Calero; Sanchez-Puelles; Villanueva; Somoza. Multifunctional Albumin-Stabilized Gold Nanoclusters for the Reduction of Cancer Stem Cells. *Cancers* **2019**, *11* (7), 969.
- (93) Camacho, K. M.; Kumar, S.; Menegatti, S.; Vogus, D. R.; Anselmo, A. C.; Mitragotri, S. Synergistic Antitumor Activity of Camptothecin-Doxorubicin Combinations and Their Conjugates with Hyaluronic Acid. *J. Controlled Release* **2015**, *210*, 198–207.
- (94) El-Mageed, H. R. A.; Mustafa, F. M.; Abdel-Latif, M. K. The Ability of Gold Nanoclusters as a New Nanocarrier for D-Penicillamine Anticancer Drug: A Computational Chemistry Study. *Struct. Chem.* **2020**, *31* (2), 781–793.
- (95) Chen, T.; Xu, S.; Zhao, T.; Zhu, L.; Wei, D.; Li, Y.; Zhang, H.; Zhao, C. Gold Nanocluster-Conjugated Amphiphilic Block Copolymer for Tumor-Targeted Drug Delivery. *ACS Appl. Mater. Interfaces* **2012**, *4* (11), 5766–5774.
- (96) Muthu, M. S.; Kutty, R. V.; Luo, Z.; Xie, J.; Feng, S. S. Theranostic Vitamin E TPGS Micelles of Transferrin Conjugation for Targeted Co-Delivery of Docetaxel and Ultra Bright Gold Nanoclusters. *Biomaterials* **2015**, *39*, 234–248.
- (97) Croissant, J. G.; Zhang, D.; Alsaïari, S.; Lu, J.; Deng, L.; Tamanoi, F.; Almalik, A. M.; Zink, J. I.; Khashab, N. M. Protein-Gold Clusters-Capped Mesoporous Silica Nanoparticles for High Drug

- Loading, Autonomous Gemcitabine/Doxorubicin Co-Delivery, and in-Vivo Tumor Imaging. *J. Controlled Release* **2016**, *229*, 183–191.
- (98) Chen, D.; Li, B.; Cai, S.; Wang, P.; Peng, S.; Sheng, Y.; He, Y.; Gu, Y.; Chen, H. Dual Targeting Luminescent Gold Nanoclusters for Tumor Imaging and Deep Tissue Therapy. *Biomaterials* **2016**, *100*, 1–16.
- (99) Lei, Y.; Tang, L.; Xie, Y.; Xianyu, Y.; Zhang, L.; Wang, P.; Hamada, Y.; Jiang, K.; Zheng, W.; Jiang, X. Gold Nanoclusters-Assisted Delivery of NGF siRNA for Effective Treatment of Pancreatic Cancer. *Nat. Commun.* **2017**, *8* (1), 1–15.
- (100) Jiang, X.; Du, B.; Huang, Y.; Yu, M.; Zheng, J. Cancer Photothermal Therapy with ICG-Conjugated Gold Nanoclusters. *Bioconjugate Chem.* **2020**, *31* (5), 1522–1528.
- (101) Zhou, F.; Feng, B.; Yu, H.; Wang, D.; Wang, T.; Liu, J.; Meng, Q.; Wang, S.; Zhang, P.; Zhang, Z.; Li, Y. Cisplatin Prodrug-Conjugated Gold Nanocluster for Fluorescence Imaging and Targeted Therapy of the Breast Cancer. *Theranostics* **2016**, *6* (5), 679–687.
- (102) Khandelia, R.; Bhandari, S.; Pan, U. N.; Ghosh, S. S.; Chattopadhyay, A. Gold Nanocluster Embedded Albumin Nanoparticles for Two-Photon Imaging of Cancer Cells Accompanying Drug Delivery. *Small* **2015**, *11* (33), 4075–4081.
- (103) Kumar, B. N. P.; Puvvada, N.; Rajput, S.; Sarkar, S.; Mahto, M. K.; Yallapu, M. M.; Pathak, A.; Emdad, L.; Das, S. K.; Reis, R. L.; Kundu, S. C.; Fisher, P. B.; Mandal, M. Targeting of EGFR, VEGFR2, and Akt by Engineered Dual Drug Encapsulated Mesoporous Silica-Gold Nanoclusters Sensitizes Tamoxifen-Resistant Breast Cancer. *Mol. Pharmaceutics* **2018**, *15* (7), 2698–2713.
- (104) Wang, M.; Wang, L.; Feng, H.; Jiang, H.; Zhou, J.; Wang, X. Precise Therapeutic Effect of Self-Assembling Gold Nanocluster-PTEN Complexes on an Orthotropic Model of Liver Cancer. *J. Cancer Res. Clin. Oncol.* **2020**, *146* (4), 875–882.
- (105) Yang, Y.; Wang, S.; Wang, C.; Tian, C.; Shen, Y.; Zhu, M. Engineered Targeted Hyaluronic Acid–Glutathione-Stabilized Gold Nanoclusters/Graphene Oxide–5-Fluorouracil as a Smart Theranostic Platform for Stimulus-Controlled Fluorescence Imaging-Assisted Synergetic Chemo/Phototherapy. *Chem. - Asian J.* **2019**, *14* (9), 1418–1423.
- (106) Wang, M.; Yu, Z.; Feng, H.; Wang, J.; Wang, L.; Zhang, Y.; Yin, L.; Du, Y.; Jiang, H.; Wang, X.; Zhou, J. In Situ Biosynthesized Gold Nanoclusters Inhibiting Cancer Development via the PI3K-AKT Signaling Pathway. *J. Mater. Chem. B* **2019**, *7* (35), 5336–5344.
- (107) Fernández, T. D.; Pearson, J. R.; Leal, M. P.; Torres, M. J.; Blanca, M.; Mayorga, C.; Le Guével, X. Intracellular Accumulation and Immunological Properties of Fluorescent Gold Nanoclusters in Human Dendritic Cells. *Biomaterials* **2015**, *43* (1), 1–12.
- (108) Tao, Y.; Ju, E.; Li, Z.; Ren, J.; Qu, X. Engineered CpG-Antigen Conjugates Protected Gold Nanoclusters as Smart Self-Vaccines for Enhanced Immune Response and Cell Imaging. *Adv. Funct. Mater.* **2014**, *24* (7), 1004–1010.
- (109) Tao, Y.; Zhang, Y.; Ju, E.; Ren, H.; Ren, J. Gold Nanocluster-Based Vaccines for Dual-Delivery of Antigens and Immunostimulatory Oligonucleotides. *Nanoscale* **2015**, *7* (29), 12419–12426.
- (110) Wang, H.; Ding, Y.; Su, S.; Meng, D.; Mujeeb, A.; Wu, Y.; Nie, G. Assembly of Hepatitis e Vaccine by 'In Situ' Growth of Gold Clusters as Nano-Adjuvants: An Efficient Way to Enhance the Immune Responses of Vaccination. *Nanoscale Horizons* **2016**, *1* (5), 394–398.
- (111) Xie, Y.; Zheng, W.; Jiang, X. Near-Infrared Light-Activated Phototherapy by Gold Nanoclusters for Dispersing Biofilms. *ACS Appl. Mater. Interfaces* **2020**, *12* (8), 9041–9049.
- (112) Zheng, K.; Setyawati, M. I.; Leong, D. T.; Xie, J. Antimicrobial Gold Nanoclusters. *ACS Nano* **2017**, *11* (7), 6904–6910.
- (113) Xie, Y.; Liu, Y.; Yang, J.; Liu, Y.; Hu, F.; Zhu, K.; Jiang, X. Gold Nanoclusters for Targeting Methicillin-Resistant *Staphylococcus Aureus* In Vivo. *Angew. Chem., Int. Ed.* **2018**, *57* (15), 3958–3962.
- (114) Xie, Y.; Zhang, M.; Zhang, W.; Liu, X.; Zheng, W.; Jiang, X. Gold Nanoclusters-Coated Orthodontic Devices Can Inhibit the Formation of Streptococcus Mutans Biofilm. *ACS Biomater. Sci. Eng.* **2020**, *6* (2), 1239–1246.
- (115) Ndigire, W.; Raviranga, N. G. H.; Lao, J.; Ramström, O.; Yan, M. Gold Nanoclusters as Nanoantibiotic Auranofin Analogues. *Adv. Healthcare Mater.* **2021**, *2101032*, 2101032.
- (116) Xiao, L.; Wei, F.; Zhou, Y.; Anderson, G. J.; Frazer, D. M.; Lim, Y. C.; Liu, T.; Xiao, Y. Dihydroliipoic Acid-Gold Nanoclusters Regulate Microglial Polarization and Have the Potential To Alter Neurogenesis. *Nano Lett.* **2020**, *20* (1), 478–495.
- (117) Gao, G.; Chen, R.; He, M.; Li, J.; Wang, L.; Sun, T. Gold Nanoclusters for Parkinson's Disease Treatment. *Biomaterials* **2019**, *194*, 36–46.
- (118) Singh, P.; Pandit, S.; Mokkalapati, V. R. S. S.; Garg, A.; Ravikumar, V.; Mijakovic, I. Gold Nanoparticles in Diagnostics and Therapeutics for Human Cancer. *Int. J. Mol. Sci.* **2018**, *19* (7), 1979.
- (119) Tsvirkun, D.; Ben-Nun, Y.; Merquiol, E.; Zlotver, I.; Meir, K.; Weiss-Sadan, T.; Matok, I.; Popovtzer, R.; Blum, G. CT Imaging of Enzymatic Activity in Cancer Using Covalent Probes Reveal a Size-Dependent Pattern. *J. Am. Chem. Soc.* **2018**, *140* (38), 12010–12020.
- (120) Zheng, K.; Xie, J. Cluster Materials as Traceable Antibacterial Agents. *Accounts Mater. Res.* **2021**, *2*, 1104.
- (121) Gao, X.; Cui, Y.; Levenson, R. M.; Chung, L. W. K.; Nie, S. In Vivo Cancer Targeting and Imaging with Semiconductor Quantum Dots. *Nat. Biotechnol.* **2004**, *22* (8), 969–976.
- (122) Smith, A. M.; Mancini, M. C.; Nie, S. Bioimaging: Second Window for in Vivo Imaging. *Nat. Nanotechnol.* **2009**, *4* (11), 710–711.
- (123) Zhao, J.; Chen, J.; Ma, S.; Liu, Q.; Huang, L.; Chen, X.; Lou, K.; Wang, W. Recent Developments in Multimodality Fluorescence Imaging Probes. *Acta Pharmaceutica Sinica B* **2018**, *8*, 320–338.
- (124) Liu, R.; Xu, Y.; Xu, K.; Dai, Z. Current Trends and Key Considerations in the Clinical Translation of Targeted Fluorescent Probes for Intraoperative Navigation. *Aggregate* **2021**, *2* (3), 1–23.
- (125) Hemmer, E.; Benayas, A.; Légare, F.; Vetrone, F. Exploiting the Biological Windows: Current Perspectives on Fluorescent Bioprobes Emitting above 1000 Nm. *Nanoscale Horizons* **2016**, *1* (3), 168–184.
- (126) Ma, Y.; Fu, H.; Zhang, C.; Cheng, S.; Gao, J.; Wang, Z.; Jin, W.; Conde, J.; Cui, D. Chiral Antioxidant-Based Gold Nanoclusters Reprogram DNA Epigenetic Patterns. *Sci. Rep.* **2016**, *6* (1), 1–12.
- (127) Genji Srinivasulu, Y.; Yao, Q.; Goswami, N.; Xie, J. Interfacial Engineering of Gold Nanoclusters for Biomedical Applications. *Mater. Horiz.* **2020**, *7* (10), 2596–2618.
- (128) Su, D.; Gao, L.; Gao, F.; Zhang, X.; Gao, X. Peptide and Protein Modified Metal Clusters for Cancer Diagnostics. *Chem. Sci.* **2020**, *11* (22), 5614–5629.
- (129) Cifuentes-Rius, A.; Deepagan, V. G.; Xie, J.; Voelcker, N. H. Bright Future of Gold Nanoclusters in Theranostics. *ACS Appl. Mater. Interfaces* **2021**, *13* (42), 49581–49588.
- (130) Zheng, K.; Xie, J. Engineering Ultrasmall Metal Nanoclusters as Promising Theranostic Agents. *Trends Chem.* **2020**, *2* (7), 665–679.
- (131) Xiao, Y.; Wu, Z.; Yao, Q.; Xie, J. Luminescent Metal Nanoclusters: Biosensing Strategies and Bioimaging Applications. *Aggregate* **2021**, *2* (1), 114–132.
- (132) Zare, I.; Chevrier, D. M.; Cifuentes-Rius, A.; Moradi, N.; Xianyu, Y.; Ghosh, S.; Trapiella-Alfonso, L.; Tian, Y.; Shourangiz-Haghighi, A.; Mukherjee, S.; Fan, K.; Hamblin, M. R. Protein-Protected Metal Nanoclusters as Diagnostic and Therapeutic Platforms for Biomedical Applications. *Mater. Today* **2021**, DOI: 10.1016/j.mattod.2020.10.027.